Electronic Supplementary Information

C-H Activation and Nucleophilic Substitution in a Photochemically Generated High Valent Iron Complex

Jia Hui Lim,[ab] Xenia Engelmann,[c] Sacha Corby,[bd] Rakesh Ganguly,[b] Kallol Ray,*[c] and Han Sen Soo*[bef]

[a] Energy Research Institute@NTU (ERI@N), Interdisciplinary Graduate School, Nanyang Technological University, Research Techno Plaza, Singapore 637553.

[b] Division of Chemistry and Biological Chemistry, School of Physical and Mathematical Sciences, Nanyang Technological University, 21 Nanyang Link, Singapore 637371.

[c] Humboldt-Universität zu Berlin, Institut für Chemie, Brook-Taylor-Straβe 2, 12489 Berlin, Germany.

[d] Imperial College London, Department of Chemistry, South Kensington Campus, London, SW7 2AZ, United Kingdom.

[e] Singapore-Berkeley Research Initiative for Sustainable Energy (SinBeRISE), 1 Create Way, Singapore 138602.

[f] Solar Fuels Laboratory, Nanyang Technological University, 50 Nanyang Avenue, Singapore 639798.

E-mail: hansen@ntu.edu.sg; kallol.ray@chemie.hu-berlin.de

Synthesis of 1

The procedures were adopted and modified from both Ellis *et. al.* and Sullivan *et. al.*.[1,2] The synthetic route is illustrated in **Fig. S1**.

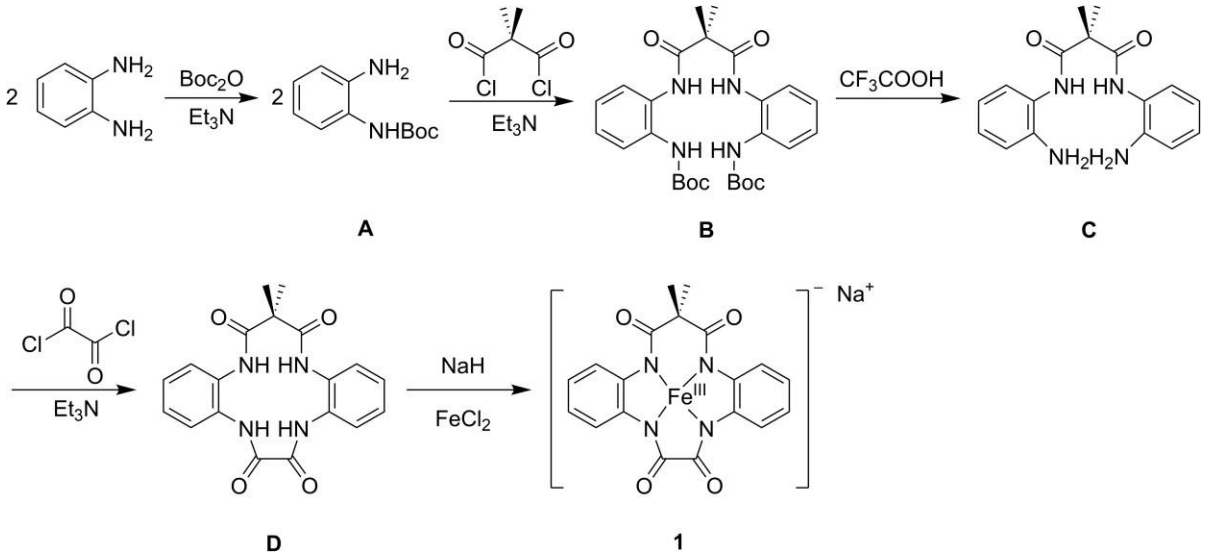

Fig. S1. Synthetic route of **1**.

Tert-butyl (2-aminophenyl)carbamate (A)

Compound 1,2-phenylenediamine (1.73 g, 16.0 mmol) was added to a three-neck round bottom flask connected to a dropping funnel and was dissolved in 75 mL anhydrous tetrahydrofuran (THF). Anhydrous Et_3N (1.8 mL, 15 mmol) was injected into the solution. Di-tert-butyl dicarbonate (Boc_2O) (3.32 g, 15.2 mmol) was dissolved in anhydrous THF (25 mL) and transferred into the dropping funnel. The Boc_2O solution was added dropwise into the 1,2-phenylenediamine solution and the reaction mixture was stirred overnight. The solvent was removed by rotary evaporation to give a viscous yellow liquid. The liquid was then suspended in pH 10 sodium bicarbonate solution ($NaHCO_3$; 50 mL) and extracted with 3 x 50 mL dichloromethane (DCM). The organic fractions were combined and rinsed with saturated $NaHCO_3$ solution (100 mL). The combined organic fractions were dried over anhydrous sodium carbonate (Na_2CO_3) and filtered. The DCM was removed by rotary evaporation to yield a pale brown oil. The oil was recrystallised with chloroform ($CHCl_3$)/hexane at 4 °C to give colourless crystals of **A** (1.49 g, 47%). ^{1}H NMR (DMSO–d_6, 500 MHz, **Fig. S20**): δ = 1.45 (s, 9 H, ^{t}Bu), 4.80 (s, 2 H, N**H**$_2$), 6.52 (m, 1 H, Ar**H**), 6.66 (m, 1 H, Ar**H**), 6.82 (m, 1 H, Ar**H**), 7.17 (m, 1 H, Ar**H**), 8.26 (br, s, 1 H, CON**H**Boc) ppm. ^{13}C NMR (DMSO–d_6, 100 MHz): δ = 28.1, 78.6, 115.7, 116.3, 123.7, 124.5, 124.9, 141.2, 153.6 ppm. HR-MS (ESI+, m/z) calculated for $C_{11}H_{16}N_2O_2$ $[M + H]^+$ *m/z* = 209.1290, found 209.1282.

Di-*tert*-butyl (((2,2-dimethylmalonyl)bis(azanediyl))bis(2,1-phenylene))dicarbamate (B)

Compound **A** (1.49 g, 7.16 mmol) was added into a three-neck round bottom flask connected to a dropping funnel and was dissolved in anhydrous THF (36 mL), after which anhydrous Et_3N (1.05 mL, 7.52 mmol) was added. Dimethylmalonyl dichloride (0.50 mL, 3.8 mmol) was added to the dropping funnel containing anhydrous THF (36 mL). The flask was cooled to 0 °C. Dimethylmalonyl dichloride solution was added to the flask at a rate of 1 drop/second. After the addition was complete, the solution was warmed up to room temperature and stirred overnight. The chalky suspension was dried by rotary evaporation. The dried product was suspended in pH 10 $NaHCO_3$ solution (30 mL) and extracted three times with DCM (30 mL each). The organic fractions were combined and rinsed with saturated $NaHCO_3$ solution (60 mL). The organic layer was dried over anhydrous Na_2CO_3 and filtered. The filtrate was dried by rotary evaporation and recrystallised in $CHCl_3$/diethyl ether (Et_2O) to yield a white solid **B** (1.25 g, 68%). ^{1}H NMR (DMSO–d_6, 500 MHz, **Fig. S21**): δ = 1.43 (s, 18 H, ^{t}Bu), 1.56 (s, 6 H, C**H**$_3$), 7.11 - 7.17 (m, 4 H, Ar**H**), 7.46 – 7.52 (m, 4 H, Ar**H**), 8.70 (br, s, 2 H, CON**H**Boc), 9.28 (br, s, 2 H, CON**H**) ppm. ^{13}C{^{1}H} NMR (DMSO–d_6, 100 MHz): δ = 23.3, 28.0, 51.0, 79.5, 123.5, 124.1, 125.7, 126.1, 129.7, 131.7, 153.7, 172.1 ppm. HR-MS (ESI+, m/z) calculated for $C_{27}H_{36}N_4O_6$ $[M + H]^+$ m/z = 513.2713, found 513.2709.

N^1,N^3-bis(2-aminophenyl)-2,2-dimethylmalonamide (C)

Compound **B** (1.25 g, 2.44 mmol) was added into a round bottom flask connected to a dropping funnel and was dissolved in DCM (7.5 mL). Trifluoroacetic acid (TFA, 7.5 mL, 98 mmol) was added to the dropping funnel containing DCM (15 mL). The flask was cooled to 0 °C. TFA solution was added to the flask at a rate of 1 drop/second. After the addition was completed, the solution was warmed up to room temperature and stirred for two hours. The solvent of the resulting solution was removed by rotary evaporation to give a yellow oil. The oil was diluted with pH 10 $NaHCO_3$ solution (20 mL) and extracted three times with DCM (20 mL each). The organic fractions were combined and rinsed with saturated $NaHCO_3$ solution (40 mL). The organic layer was dried over anhydrous Na_2CO_3 and filtered. The filtrate was dried by rotary evaporation to give a white solid **C** (0.555 g, 73%). ^{1}H NMR (DMSO–d_6, 500 MHz, **Fig. S22**): δ = 1.57 (s, 6 H, C**H**$_3$), 4.91 (br, s, 4 H, N**H**$_2$), 6.54 (m, 2 H, Ar**H**), 6.71 (m, 2 H, Ar**H**), 6.94 – 6.98 (m, 4H, Ar**H**), 9.00 (br, s, 2 H, CON**H**) ppm. ^{13}C{^{1}H} NMR (DMSO–d_6, 100 MHz): δ = 23.5, 50.7, 115.4, 115.9, 122.7, 126.9, 127.5, 144.1, 172.8 ppm. HR-MS (ESI+, m/z) calculated for $C_{17}H_{20}N_4O_2$ $[M + H]^+$ m/z = 313.1665, found 313.1663.

Compound 15,15-dimethyl-8,13-dihydro-5H-dibenzo[b,h][1,4,7,10]tetraazacyclotridecine-6,7,14,16(15H,17H)-tetraone (D)

Compound **C** (0.490 g, 1.57 mmol) was added into a three-neck round bottom flask connected to a dropping funnel and was dissolved in anhydrous THF (770 mL). Oxalyl chloride solution (0.87 mL of a 2 M solution, 1.7 mmol) was injected into the anhydrous THF (175 mL) in the dropping funnel. Anhydrous Et_3N (0.46 mL, 3.3 mmol) was then added into the solution in the flask. The flask was cooled to 0 °C. Oxalyl chloride solution was added to the flask at a rate of 1 drop/second. After the addition was completed, the cloudy solution was warmed up to room temperature and stirred overnight. Removal of the solvent by rotary evaporation gave a pale yellow solid. The solid was suspended in deionised water (100 mL) and sonicated before being filtered off. The residue was washed with copious amounts of deionised water and then sonicated in Et_2O. The resulting residue was dried *in vacuo* to give a white solid **D** (0.489 g, 85%). ^{1}H NMR (DMSO–d_6, 500 MHz, **Fig. S23**): δ = 1.55 (s, 6 H, C**H**$_3$), 7.27 – 7.37 (m, 6 H, Ar**H**), 7.60 – 7.61 (m, 2 H, Ar**H**), 9.54 (br, s, 2 H, CON**H**), 9.64 (br, s, 2 H, CON**H**) ppm. ^{13}C{^{1}H} NMR (DMSO–d_6, 100 MHz): δ = 23.3, 51.2, 125.5, 126.0, 126.5, 127.2, 130.8, 131.7, 161.9, 172.5 ppm. HR-MS (ESI-, m/z) calculated for $C_{19}H_{18}N_4O_4$ [M - H]$^-$ *m/z* = 365.1250, found 365.1258.

Sodium salt of 1

Compound **D** (0.489 g, 1.33 mmol) was added into a Schlenk flask and was suspended in anhydrous THF (75 mL). NaH (60% in mineral oil, 234 mg, 5.85 mmol) was subsequently added to the solution and the mixture was stirred vigorously for 15 minutes until the suspension turned to a pale yellow cloudy suspension. Iron (II) chloride (211 mg, 1.66 mmol) was added into the solution and the reaction mixture was stirred overnight, resulting in a brown-green suspension. Exposure of the solution to air caused the suspension to turn brown. The suspension was then filtered to give a dark brown filtrate and a dark brown residue, which were worked up separately to give two crops of product. The first crop was obtained by adding the filtrate into pentane (300 mL), giving rise to the formation of brown precipitate. The precipitate was filtered off, dissolved in methanol (MeOH), and dried by rotary evaporation to give a reddish brown crystalline solid. The second crop was obtained by dissolving the residue in MeOH (3 x 5 mL) and filtered. The filtrate was collected and its solvent removed by rotary evaporation, giving a reddish brown crystalline solid. The combined yield from both crops was 513 mg (84%). For cyclic voltametric and transient absorption spectroscopic experiments, further purification using C-18 reverse-phase preparative column chromatography (Merck LiChroprep ®RP-18, 40 – 63 μm) was required. The Na salt of **1** (100 mg) was dissolved in 3 mL of ultrapure water and introduced into the column. The orange band observed was eluted with 25% MeOH in ultrapure water. The column should be completed within an hour to minimise degradation of the Na salt of **1** in the column.

Alternatively, cation metathesis could also be performed on the Na salt of **1** to form the PPh_4 salt as the purification step. HR-MS (ESI-, m/z) calculated for $C_{19}H_{14}N_4NaO_4^-$ *m/z* = 418.0364, found 418.0362.

PPh_4 salt of 1

The Na salt of **1** (100 mg, 0.22 mmol) was dissolved in ultrapure water (10 mL) to give a red solution. Tetraphenylphosphonium chloride (PPh_4Cl, 412 mg, 1.1 mmol) was added as a solid into the solution and sonicated for 30 seconds, resulting in an orange suspension. The suspension was filtered and the residue was rinsed with ultrapure water (30 mL). The residue was then dissolved in MeOH and dried by rotary evaporation to give a reddish brown solid.

Mössbauer Spectroscopy

The synthesis of $^{57}FeCl_2$ was adapted from *Inorganic Syntheses*.[3] Metallic ^{57}Fe (Isoflex USA, 95.78% enriched, 10 mg, 0.18 mmol) was added to a 10 mL Schlenk flask and was suspended in anhydrous MeOH (1 mL). Concentrated hydrochloric acid (~12 M, 40 μL, ~0.48 mmol) was added to the suspension. The mixture was bubbled with N_2 for 5 minutes. The Schlenk flask was sealed and heated at 100 °C for 3 hours. The resulting light green suspension was worked up by Schlenk filtration. The residue was washed with anhydrous MeOH (3 x 1 mL), filtered, and the combined organic phases were dried *in vacuo* to give an off-white solid. The solid was then dried further *in vacuo* at 100 °C for 4 hours to yield $^{57}FeCl_2$ as a beige powder. The PPh_4^+ salt of **^{57}1** was synthesised by employing the same procedure as that for the PPh_4^+ salt of **1**, but with $^{57}FeCl_2$ being the limiting reagent. The Mössbauer data and fits are shown in **Figure 6** (Main Text) and **Fig. S2**, and their quadrupole splittings (ΔE_Q) and isomer shifts (δ) are summarised in **Table 2** (Main Text).

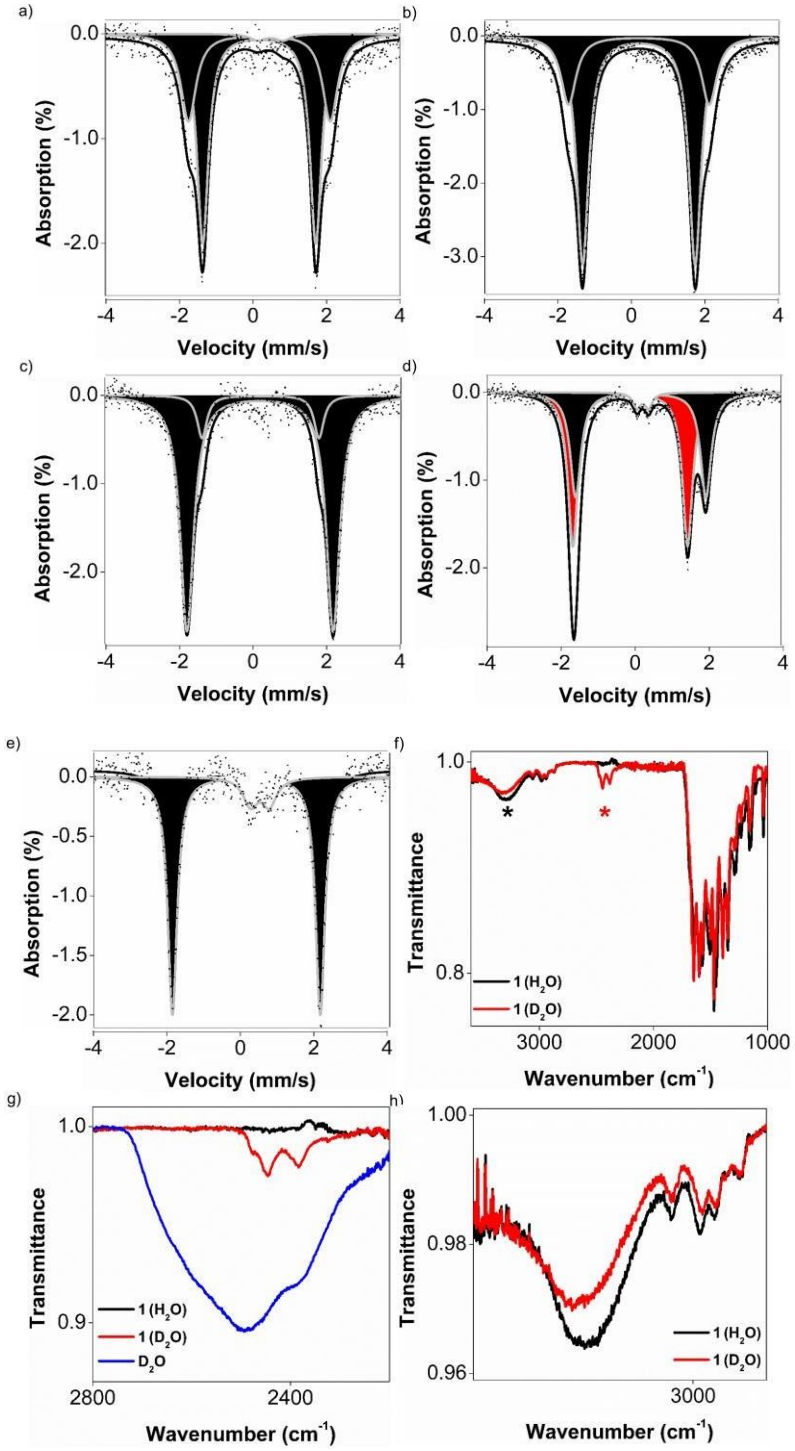

Fig. S2. Mössbauer spectra of (a) 2 mM solution of ^{57}**1** in 1:1 water:acetonitrile, (b) 2 mM solution of ^{57}**1** in acetonitrile, (c) solid **1**, (d) 2 mM solution of ^{57}**1** + $Ru^{III}(bpy)_3^{3+}$ (4 eq.) + Cl^- (10 eq.) in 1:1 water:acetonitrile, stirred at room temperature for 30 mins, and (e) 2 mM solution of ^{57}**1** + $Ru^{III}(bpy)_3^{3+}$ (4 eq.) + Br^- (10 eq.) in 1:1 water:acetonitrile, stirred at room temperature for 90 mins. The black lines are the spectral simulations representing >95% of the absorption. The shaded areas are the spectral contributions from $^{57}Fe^{III}$ (black) and ^{57}**1**$^+$ (red). A high-spin Fe^{III} impurity (5-10%) that we attribute to a deligated by-product, is observed in all cases. (f) Infrared spectra of **1** (black) and **1** after exchange with D_2O (red). Regions containing infrared bands of interest are marked with *****. (g) Region containing O-D stretch (***** in **Fig. S2f**), with infrared signals from pristine D_2O (blue). (h) Region containing O-H stretch (***** in **Fig. S2f**).

In all of the Mössbauer spectra, there is a small contribution of ^{57}Fe species with ΔE_Q (0.3 – 0.7 mm s^{-1}) and δ (0.2 – 0.5 mm s^{-1}) that is not consistent with any known (TAML)Fe compounds, which we propose to be the deligated (TAML)Fe (unshaded region of the Mössbauer spectra). The H^+-induced deligation of (TAML)Fe complexes by buffer salts has been reported.[4] Therefore, we hypothesise that the presence of stoichiometric or excess amounts of other reagent ions, coupled with the relatively high concentrations of **^{57}1** (2 mM in the Mössbauer experiments, in comparison to the sub-μM concentrations employed in most of the (TAML)Fe-H_2O_2 catalytic processes), have contributed to the observed deligation of **^{57}1** and its oxidised products.

For the moderately labile Cl^- nucleophile, predominantly Fe^{IV} (71 %, Main Text, **Table 2**, Entry 5, and Main Text **Figure 6c**) and some Fe^{III}(Cl)-TAML$^{\bullet+}$ (29 %, Main Text, **Table 2**, Entry 5, and **Figure 6c**) were observed. The minor **1(Cl)-TAML$^{\bullet+}$** component undergoes similar nucleophilic attack by Cl^- to give **1-TAML(Cl)$_n$** (40 %, Main Text, **Table 2**, Entry 6, and **Fig. S2b**) within 30 mins of stirring at room temperature. As **1(Cl)-TAML$^{\bullet+}$** gets consumed, the equilibrium shifts more **1$^+$(Cl)** to **1(Cl)-TAML$^{\bullet+}$** by valence-tautomerisation, slowly consuming more of the **1$^+$(Cl)** (from 71% to 56 %, Main Text, **Table 2**, Entry 6, and **Fig. S2b**). The valence tautomerisation and nucleophilic attack processes are in competition with the natural decay of **1$^+$(Cl)** (27 ± 4 mins, **Fig. S12a**), leading to only partial conversion to **1-TAML(Cl)** and **1-TAML(Cl)$_2$**.

Complex **^{57}1$^+$(CN)$_2$** (purified by recrystallisation) appeared to consist of 80% Fe^{IV} (Main Text, **Table 2**, Entry 9, and **Figure 8d**), while the remainder was probably the deligated product. We found that the purified **1$^+$(CN)$_2$** was more unstable than the crude **1$^+$(CN)$_2$** in solution, as evident by the fact that the crude **1$^+$(CN)$_2$** had a moderate stability in solution at room temperature under normal atmospheric conditions (**Fig. S18a-b**), while the purified **1$^+$(CN)$_2$** crystals decomposed rapidly outside the glovebox. The preparation of the **^{57}1$^+$-(CN)$_2$** Mössbauer sample involved dissolving the purified **^{57}1$^+$(CN)$_2$** in ACN in a glovebox and then freezing the **^{57}1$^+$(CN)$_2$** solution outside the glovebox. It appeared that **^{57}1$^+$(CN)$_2$** decomposed and underwent deligation during the short time that the **^{57}1$^+$(CN)$_2$** solution was exposed to the normal atmosphere before it was frozen.

Cyclic Voltammetry

The cyclic voltammetric features of **1** showed three quasi-reversible oxidations at $E_{1/2}$ potentials of +0.10, +0.39, and +0.63 V vs. Fc^+/Fc and irreversible reductions at -0.13 and +0.15 V (**Fig. S3**), as opposed to the single quasi-reversible wave at +0.50 V reported by Sullivan *et al.*.[2] In all subsequent discussions, the potentials are reported relative to Fc^+/Fc. We propose that the experiments in the prior study may have had deposition of the oxidised product(s) of **1** on the electrode, which we overcame by polishing the electrode after every potential sweep. Regardless, our results suggest that the oxidation of **1** by the well-characterised $Ru(bpy)_3^{2+}$ photosensitiser ($E_{Ru(III)/Ru(II)}$ ≈ +0.85 V)[6] should be thermodynamically feasible, with the formal oxidation states determined by Mössbauer spectroscopy, as reported in the Mössbauer section above.

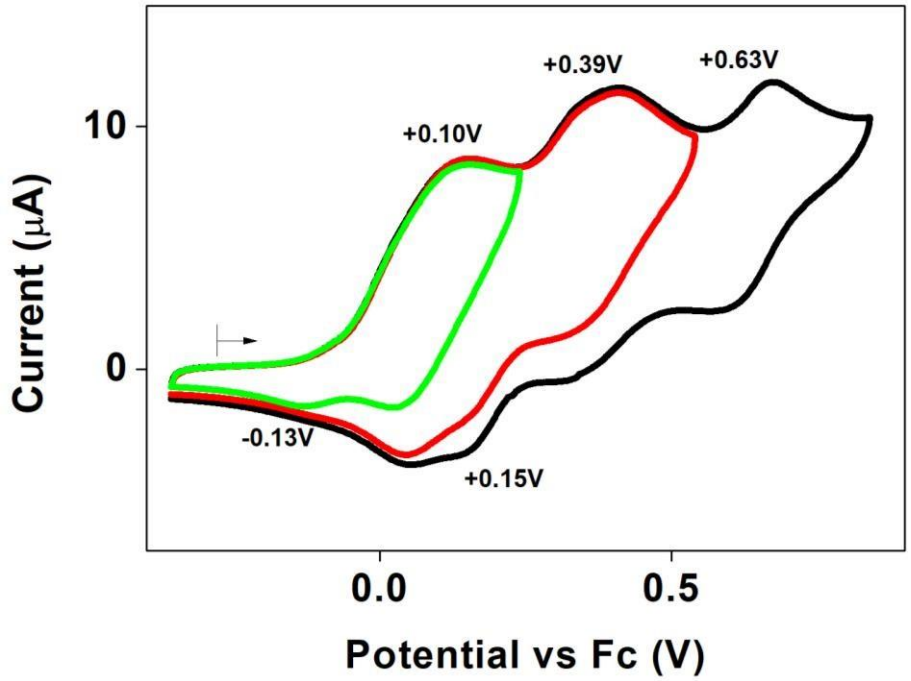

Fig. S3. Cyclic voltammograms of the Na salt of **1** over several scan ranges. The irreversible reduction peak at +0.15 V vs. Fc^+/Fc appeared only after **1** had been oxidised up to at least +0.39 V (red). Similarly, the irreversible reduction at -0.13 V appeared only if **1** had *not* been oxidised beyond +0.10 V (green). ([**1**] = 0.90 mM, [*n*-Bu_4NPF_6] = 0.10 M, glassy-carbon working electrode). Scan rate = 100 mV s^{-1}

Nanosecond Transient Absorption Spectroscopic Measurements

The detailed composition of each set of experiment is depicted in **Table S1**.

Table S1. Different conditions tested using 3 mL solutions for transient absorption measurements.

Entry	Reagents (concentration)		
	$Co(NH_3)_5Cl_3$ (10 mM)	$Ru(bpy)_3Cl_2$ (0.020 mM)	**1** (0.20 mM)
1		□	
2		□	□
3	□	□	
4	□	□	□

A control experiment with **1** alone showed that it did not exhibit any observable transient absorption signals upon laser excitation. Intriguingly, **1** partly quenched the excited state of $Ru(bpy)_3^{2+*}$ (Main Text, **Table 1**, entry 2, **Fig. S4, 5b, 6b, 7b,** and **8b**) compared to a solution containing only $Ru(bpy)_3Cl_2$ (Main Text, **Table 1**, entry 1, **Fig. S5a**, **6a**, **7a**, and **8a**), with a bimolecular rate constant of $5.3 \times 10^9\ M^{-1}s^{-1}$ (**Fig. S10a**). This may be attributed to triplet energy transfer from $Ru(bpy)_3^{2+*}$ to **1**, followed by a non-radiative decay of **1*** back to its ground state. Nevertheless, as reported previously,[7,8] $[Co(NH_3)_5Cl]^{2+}$ oxidatively quenched $Ru(bpy)_3^{2+*}$ at an even faster rate due to the high concentrations that we used (Main Text, **Table 1**, entry 3, **Fig. S5c**, **6c**, **7c**, and **8c**), despite having a lower biomolecular rate constant of $1.1 \times 10^8\ M^{-1}s^{-1}$.

The TAS signals, probed at characteristic wavelengths (365 nm, 470 nm and 730 nm) and the TES signal (600 nm) of $Ru(bpy)_3Cl_2$, are illustrated in **Fig. S5-8**, with each figure showing the transient signal of a particular probe wavelength in solutions comprising different compositions.

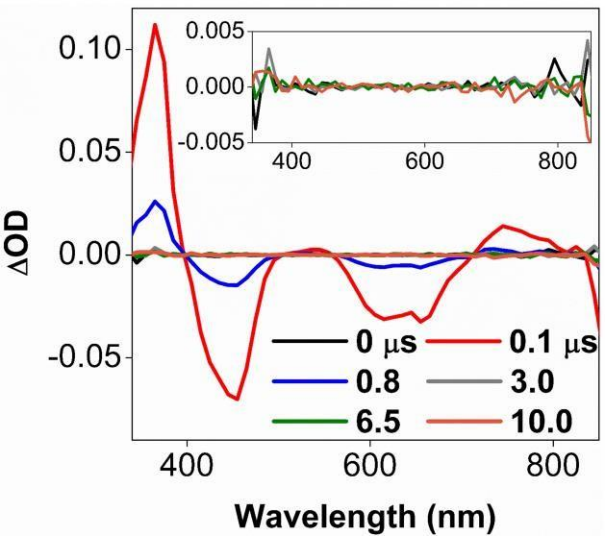

Fig. S4. TAS signals of $Ru(bpy)_3Cl_2$ (0.020 mM) + **1** (0.20 mM) (**Table S1**, Entry 2) at different times (0 – 10 μs) after laser excitation. The inset features the spectra over the same wavelengths with an expanded vertical scale, showing the TAS signals returning to the origin.

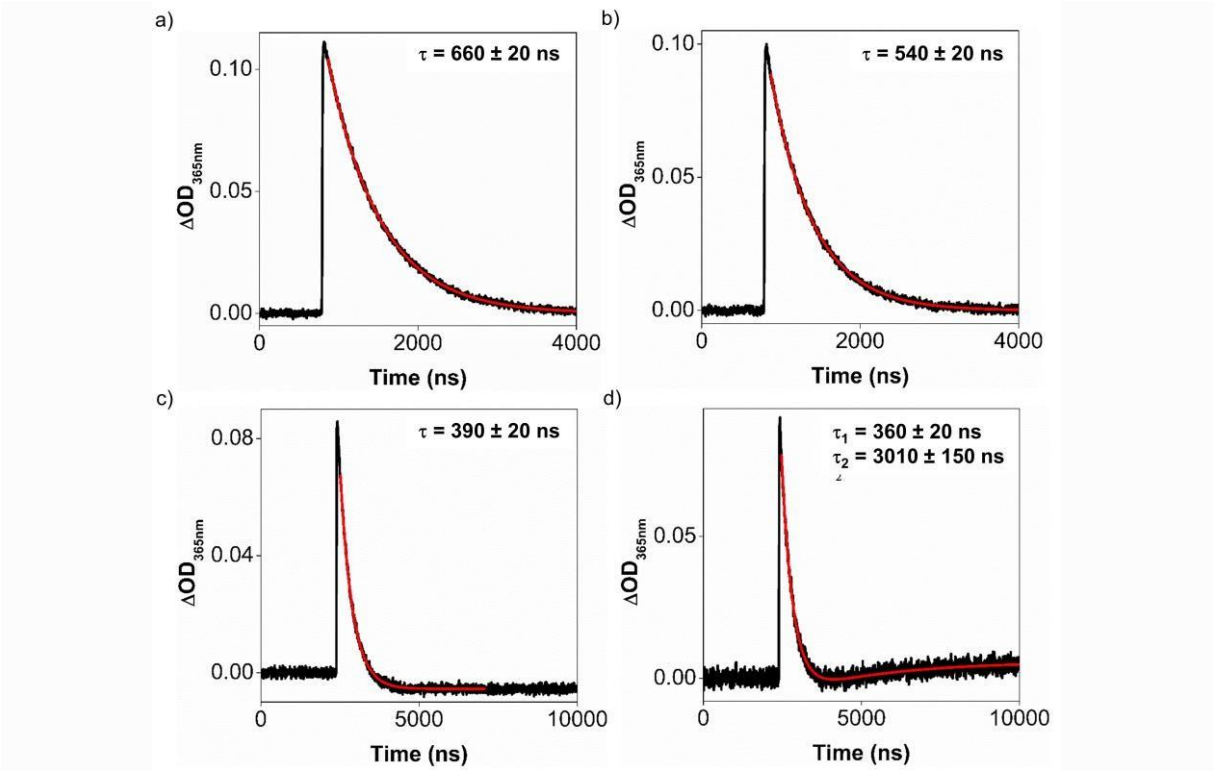

Fig. S5. TAS signals (black), probed at 365 nm, under different conditions. The fits to the kinetics are the lines in red. (a) $Ru(bpy)_3Cl_2$ only (Entry 1). (b) $Ru(bpy)_3Cl_2$ + **1** (Entry 2). (c) $Ru(bpy)_3Cl_2$ + $Co(NH_3)_5Cl_3$ (Entry 3). (d) $Ru(bpy)_3Cl_2$ + **1** + $Co(NH_3)_5Cl_3$ (Entry 4).

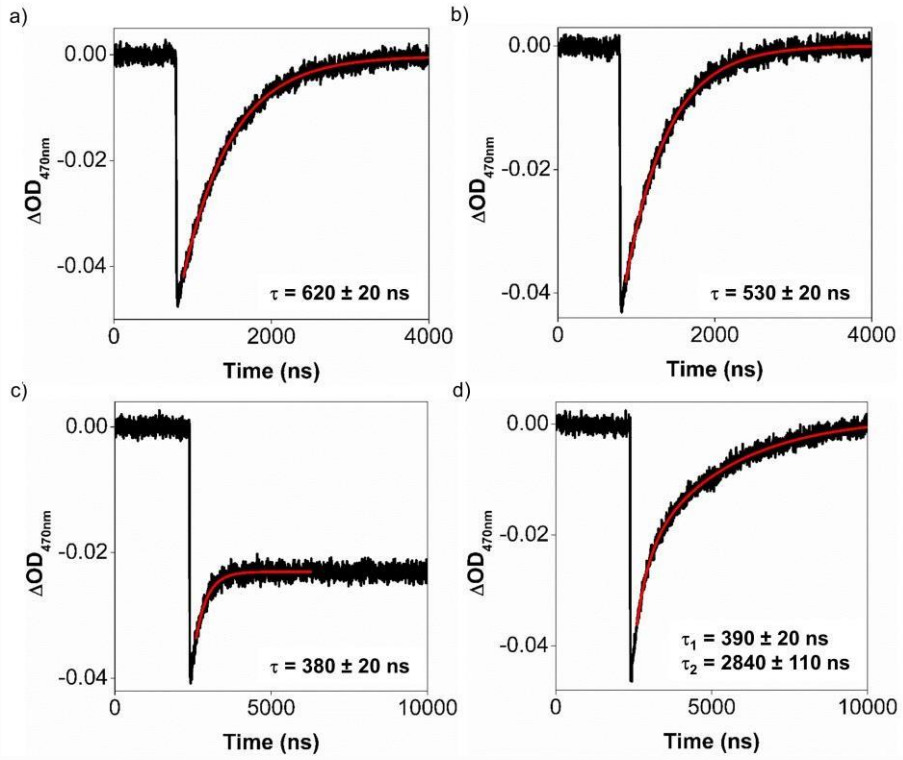

Fig. S6. TAS signals (black), probed at 470 nm, under different conditions. The fits to the kinetics are the lines in red. (a) $Ru(bpy)_3Cl_2$ only (Entry 1). (b) $Ru(bpy)_3Cl_2$ + **1** (Entry 2). (c) $Ru(bpy)_3Cl_2$ + $Co(NH_3)_5Cl_3$ (Entry 3). (d) $Ru(bpy)_3Cl_2$ + **1** + $Co(NH_3)_5Cl_3$ (Entry 4).

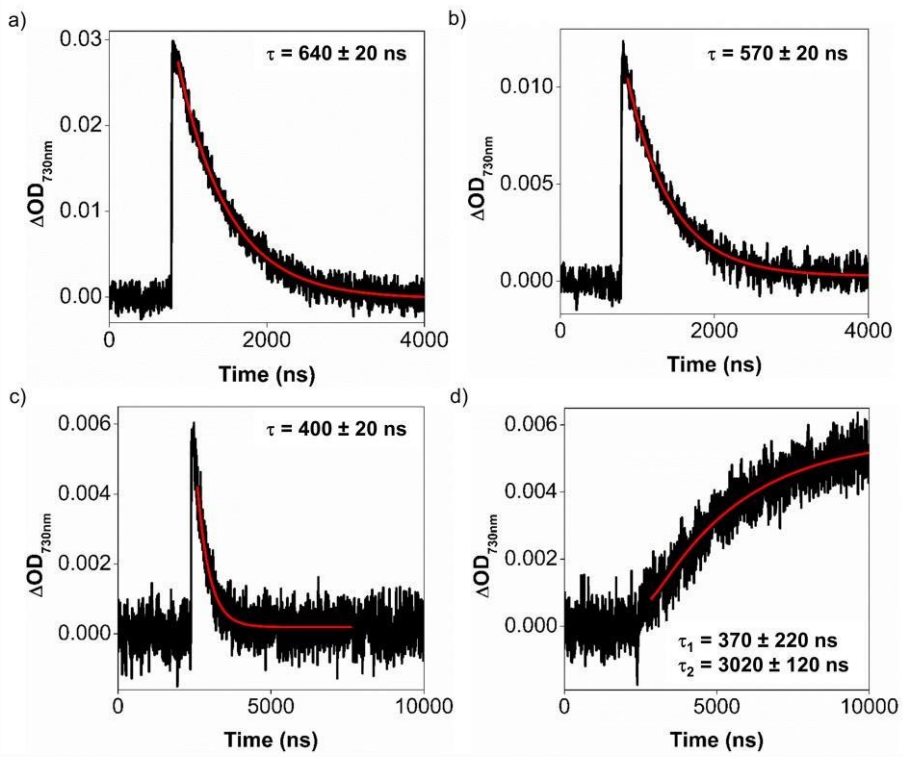

Fig. S7. TAS signals (black), probed at 730 nm, under different conditions. The fits to the kinetics are the lines in red. (a) $Ru(bpy)_3Cl_2$ only (Entry 1). (b) $Ru(bpy)_3Cl_2$ + **1** (Entry 2). (c) $Ru(bpy)_3Cl_2$ + $Co(NH_3)_5Cl_3$ (Entry 3). (d) $Ru(bpy)_3Cl_2$ + **1** + $Co(NH_3)_5Cl_3$ (Entry 4).

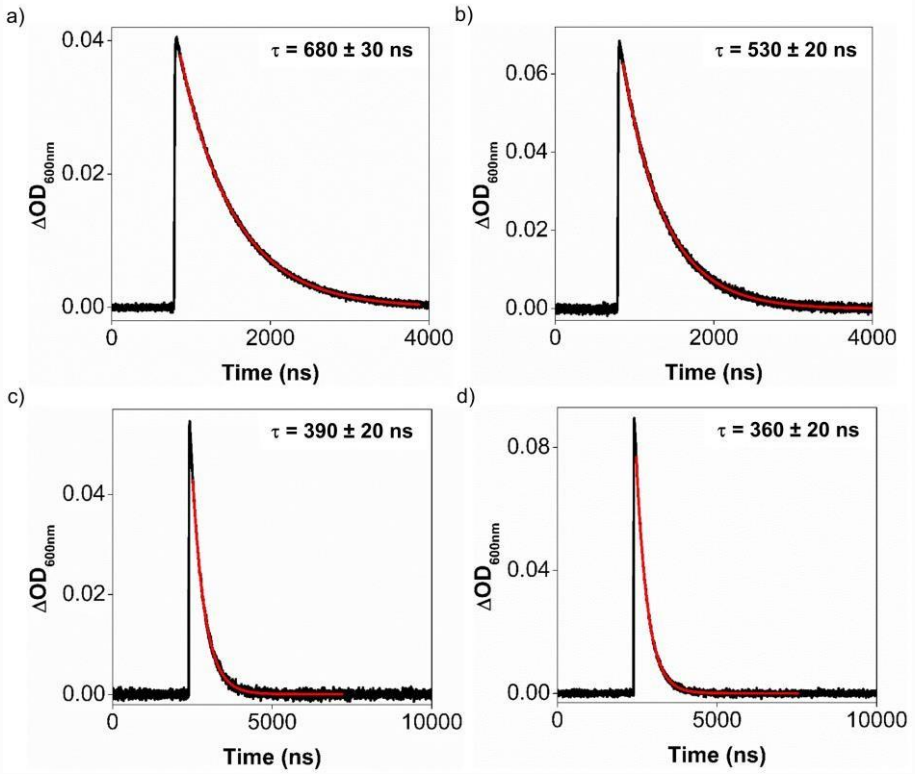

Fig. S8. Transient ***emission*** spectroscopic signals (black), probed at 600 nm, under different conditions. The fits to the kinetics are the lines in red. (a) $Ru(bpy)_3Cl_2$ only (Entry 1). (b) $Ru(bpy)_3Cl_2$ + **1** (Entry 2). (c) $Ru(bpy)_3Cl_2$ + $Co(NH_3)_5Cl_3$ (Entry 3). (d) $Ru(bpy)_3Cl_2$ + **1** + $Co(NH_3)_5Cl_3$ (Entry 4).

Determination of Bimolecular Quenching Rate Constants

The expected elementary steps following the laser excitation of $Ru(bpy)_3^{2+}$ are illustrated in **Fig. S9**.

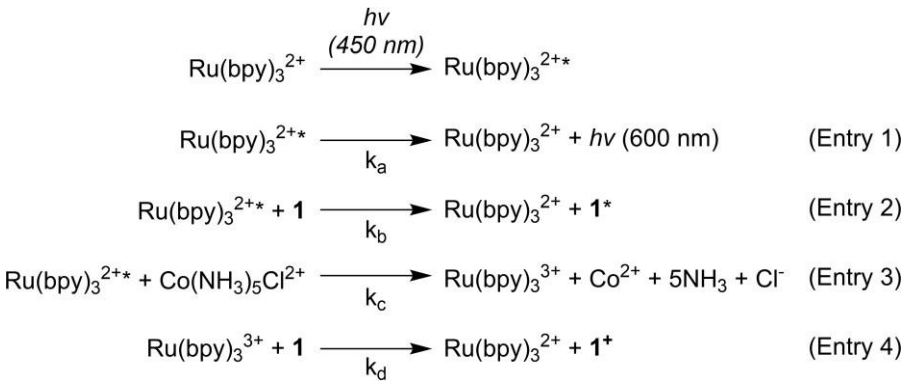

Fig. S9. Anticipated elementary steps involved after laser excitation of $Ru(bpy)_3^{2+}$.

In the absence of any quencher, $Ru(bpy)_3^{2+*}$ decays back to the ground state and has a photoluminescence band (λ_{max} = 600 nm) with a rate constant k_a (**Fig. S8a**). The bimolecular quenching rate constant, k_b, is related to the lifetime, τ_b, of $Ru(bpy)_3^{2+*}$ in the presence of **1** as the quencher (**Fig. S8b**) with a concentration of [**1**], by the Stern-Volmer equation:

$$\frac{\tau_a}{\tau_b} = 1 + k_b \tau_a [\mathbf{1}]$$

where τ_a is the lifetime of $Ru(bpy)_3^{2+*}$ in the absence of a quencher.

Photoemission lifetime at 600 nm is chosen as the reference wavelength, since it is characteristic of only $Ru(bpy)_3^{2+*}$, and is therefore free from interference from other species. The bimolecular quenching rate constant k_b was obtained by plotting τ_a/τ_b against [**1**] with a fixed vertical intercept of 1 (**Fig. S10a**). The gradient ($k_b\tau_a$) was determined to be $3.6 \pm 0.1 \times 10^3 M^{-1}$. Given that τ_a is 680 ± 30 ns (**Fig. S8a**) , k_b was subsequently calculated to be $5.3 \pm 0.1 \times 10^9\ M^{-1}s^{-1}$.

Since $Ru(bpy)_3^{3+}$ is a long-lived species, the Stern-Volmer equation can be simplified to:

$$\frac{1}{\tau_d} \approx k_d [\mathbf{1}]$$

where τ_d is the lifetime of $Ru(bpy)_3^{3+}$ in the presence of **1**, and k_d is the corresponding bimolecular hole transfer rate constant from $Ru(bpy)_3^{3+}$ to **1**.

As [**1**] increases, the rate of consumption of $Ru(bpy)_3^{3+}$ increases, resulting in a shorter lifetime τ_d. The wavelength 365 nm is chosen as the reference wavelength because at this wavelength $Ru(bpy)_3^{3+}$ has a negative ΔOD whereas $\mathbf{1}^+$ has a positive ΔOD, compared to the ground state $Ru(bpy)_3^{2+}$, thereby giving clear indication of the hole transfer from $Ru(bpy)_3^{3+}$ to **1** (**Fig. S5d**). From the biexponential fit of the transient spectroscopic signal, the longer lifetime, corresponding to the hole transfer from $Ru(bpy)_3^{3+}$ to **1**, was taken to be τ_d. A graph of $1/\tau_d$ against [**1**] was then plotted, with its vertical intercept set at 0 (**Fig. S10b**). The gradient representing k_d, was found to be $3.9 \pm 0.1 \times 10^9\ M^{-1}s^{-1}$.

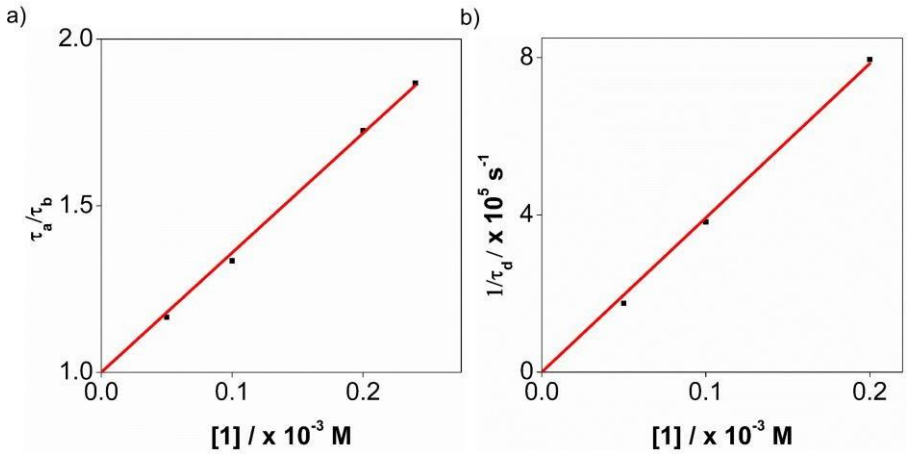

Fig. S10. (a) Stern-Volmer plot for the quenching of the transient emission signal of $Ru(bpy)_3^{2+*}$ at 600 nm by varying [**1**]. (b) Simplified Stern-Volmer plot for the quenching of the transient absorption signal of $Ru(bpy)_3^{3+}$ at 350 nm by varying [**1**].

Transient Absorption Measurements at Four-Seconds Timescale

A sample containing $Ru(bpy)_3Cl_2$ (0.020 mM), **1** (0.20 mM), and $Co(NH_3)_5Cl_3$ (10 mM) (**Table S1,** Entry 4) was probed at 600 nm and 830 nm (close to the characteristic wavelengths of the oxidised **1**). The resulting plots are illustrated in **Fig. S11**.

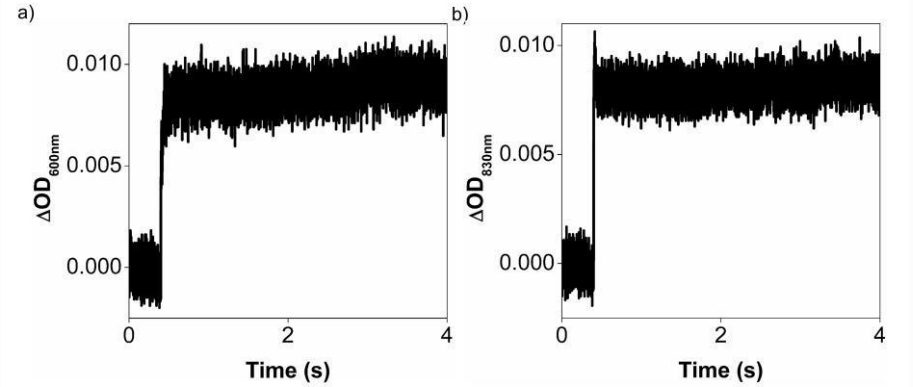

Fig. S11. TAS signals of $Ru(bpy)_3Cl_2$ (0.020 mM) + **1** (0.20 mM) + $Co(NH_3)_5Cl_3$ (10 mM), on 4-second timescales with a (a) 600 nm probe wavelength, and a (b) 830 nm probe wavelength. The data recorded at both wavelengths show that the oxidised **1** has increased absorbance compared to **1,** and the lifetime of the oxidised **1** exceeds four seconds.

Oxidation of the Sodium Salt of 1 Using Independently Generated $Ru(bpy)_3^{3+}$

The resulting spectra are shown in **Fig. S12**. The spectral features of **1** + 2 eq. $Ru(bpy)_3^{3+}$ are similar to those of **1** + 1 eq. $Ru(bpy)_3^{3+}$ (**Fig. S12b**), suggesting that the additional one equivalent of $Ru(bpy)_3^{3+}$ was probably used to oxidise **1** and overcome the intrinsic decay of the oxidised form back to its reduced state during the measurement.

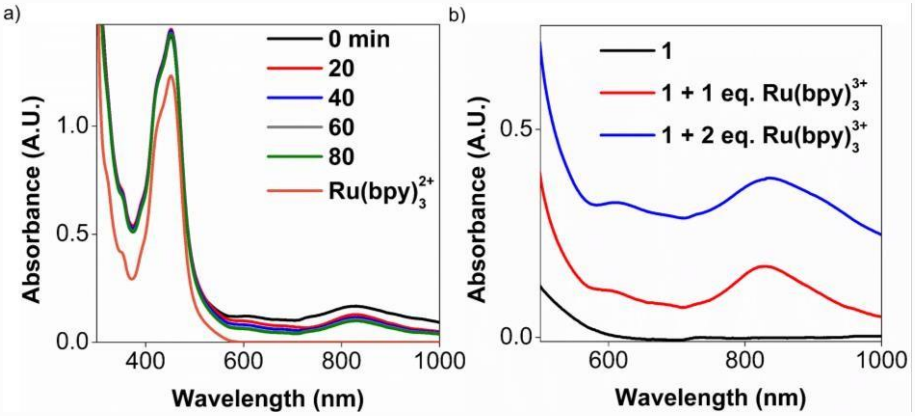

Fig. S12. (a) UV-visible spectral changes over time for the reaction between photochemically generated $Ru(bpy)_3^{3+}$ (0.10 mM, 1 equivalent) and **1** (0.10 mM). Using the absorbance at 828 nm, the lifetime of the oxidised **1** was fitted to a mono-exponential decay curve and τ_{828nm} was found to be 27 ± 4 mins. (b) Comparison of the UV-visible spectra of **1**, **1** + 1 eq. $Ru(bpy)_3^{3+}$, and **1** + 2 eq. $Ru(bpy)_3^{3+}$.

Oxidation of the Sodium Salt of 1 Using Independently Generated $(ArMe)_3N^{\bullet+}$ in the Presence of Different Nucleophiles

We chose the tri(*p*-tolyl)aminium radical-cation ($(ArMe)_3N^{\bullet+}$) as an alternative oxidant to $Ru(bpy)_3^{3+}$ due to the following reasons: (1) $(ArMe)_3N^{\bullet+}$ is also an outer-sphere oxidant similar to $Ru(bpy)_3^{3+}$; (2) the $E^{0'}_{(ArMe)3N\bullet+/(ArMe)3N}$ of +0.40 V vs Fc^+/Fc[9] is thermodynamically feasible for oxidising **1** by at least one electron (first $E_{1/2}$ potential of **1** = +0.10 vs. Fc^+/Fc, **Fig. S3**); (3) the reduced by-products, $(ArMe)_3N$ and PbO, and the excess PbO_2 oxidant, can be removed easily to give (TAML)Fe products of higher purity; (4) our new method of generating $(ArMe)_3N^{\bullet+}$ using PbO_2/HBF_4 can be conducted under partially aqueous conditions without the need for any Schlenk techniques, as opposed to the use of $NOBF_4$ as an oxidant.[10] $(ArMe)_3N$ was synthesised with slightly modified procedures described by Goodbrand and Hu.[11] The reaction scheme is shown in **Fig. S13**.

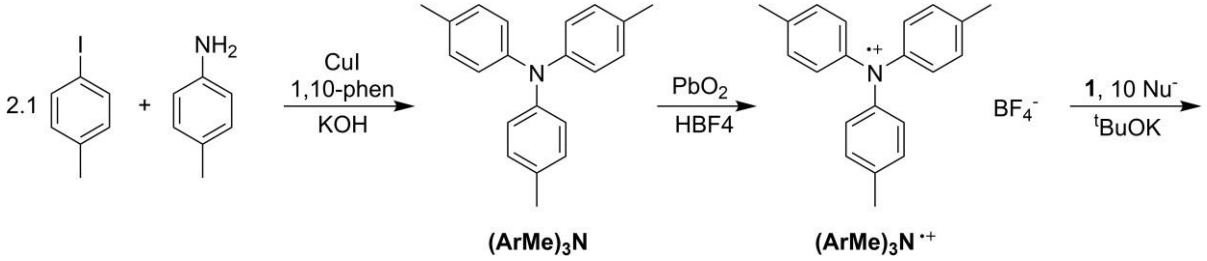

Fig. S13. Reaction scheme depicting the syntheses of $(ArMe)_3N$ and $(ArMe)_3N^{\bullet+}$, and the oxidation of **1** by $(ArMe)_3N^{\bullet+}$ in the presence of different nucleophiles. Nu^-: nucleophile.

Optimisation of the Oxidation of 1 in the Presence of Bromide as a Nucleophile

Since bromide showed the highest yield and cleanest mixture (according to ESI-MS) of a nucleophile-substituted product, **1-TAML(Br)$_2$**, this synthesis was optimised to facilitate its isolation. This reaction was monitored by negative-ion mode ESI-MS. During the optimisation process, the Na salt of **1** was found to give a higher yield of nucleophilic substitution than its PPh_4 counterpart. In addition, the presence of a base was determined to be paramount for the reaction, because the acidic HBF_4 (from the synthesis of $(ArMe)_3N^{\bullet+}$) can cause deligation of **1**. Potassium tert-butoxide (^{t}BuOK) was found to be the most suitable base. We also investigated the use of different bromide salts, i.e. tetrabutylammonium bromide (TBABr), tetraethylammonium bromide (TEABr), tetraphenylphosphonium bromide (PPh_4Br), and lithium bromide (LiBr). The counter-cation will most likely associate with [**1-TAML(Br)$_2$**]$^-$ in the substituted product, since the bromide salt is present in huge excess. The cation was found to affect the hydrolytic stability of the [**1-TAML(Br)$_2$**]$^-$ product, with TEA^+ being the most stabilising, and Li^+ being the least, the latter leading to the deligated $TAML(Br)_2$ ligand. Different reaction temperatures (0°C, 25 ºC, and 50 ºC) were also explored, of which 25 ºC was found to be best. In addition, the maximum number of Br-substitution was evaluated by systematically

increasing the equivalents of $(ArMe)_3N\bullet^+$ oxidant by two per Br-substitution. We found that the di-substitution by Br using 4 equivalents $(ArMe)_3N\bullet^+$ gave the highest selectivity for **1-TAML(Br)$_2$**, with some minor amounts of **1-TAML(Br)** and **1-TAML(Br)$_3$**. Attempts to carry out four Br-substitutions on **1** by using eight equivalents of $(ArMe)_3N\bullet^+$ gave a distribution of **1-TAML(Br)$_n$** products and the corresponding deligated counterparts (**Fig. S14a**). We propose that the combination of the steric hindrance and the electron withdrawing nature of the Br substituent in **1-TAML(Br)$_2$** leads to slower rates of Br-substitutions beyond **1-TAML(Br)$_2$**. With the optimised conditions, **1-TAML(Br)$_2$** was successfully synthesised and purified (**Fig. S14b**).

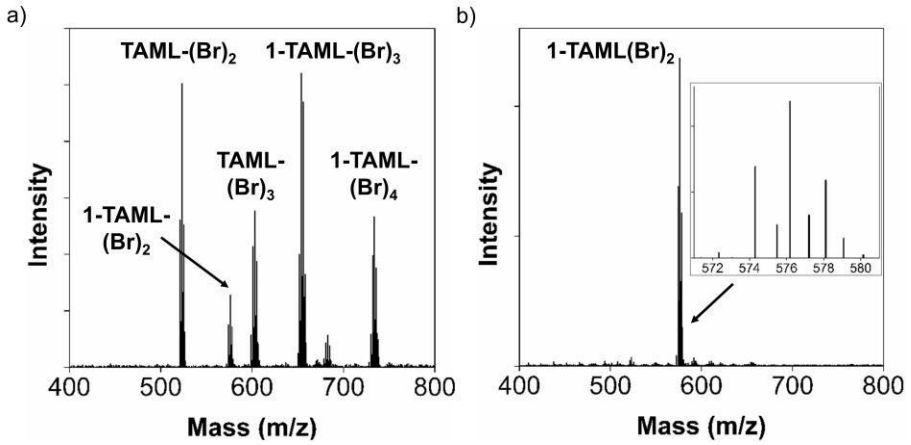

Fig. S14. Negative-ion mode ESI-MS and the assigned species in the crude reaction mixture containing **1** (1 eq), ^{t}BuOK (4.2 eq), TEABr (10 eq), and $(ArMe)_3N\bullet^+$ (8 eq). (b) Negative-ion mode ESI-MS of **1-TAML(Br)$_2$** isolated from reverse-phase column chromatography, with the isotopic distribution shown in the inset.

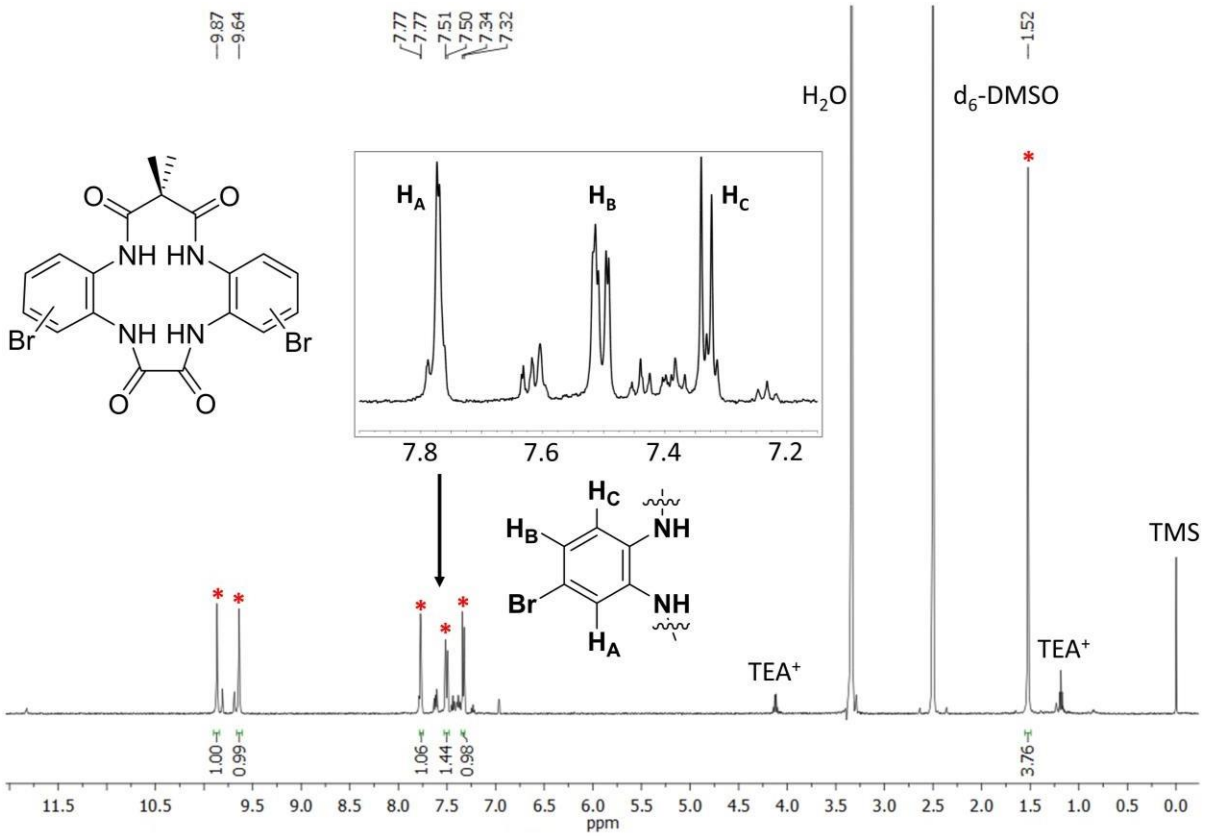

Fig. S15. The ^{1}H NMR spectrum of the TAML(Br)$_2$ ligand derived from acid hydrolysis of **1(Br)-TAML(Br)$_2$**. The NMR signals assigned to the symmetrical TAML(Br)$_2$ are marked with a red asterisk (*****). The unassigned signals are proposed to be the asymmetrically bromide-substituted TAML(Br)$_2$ or decomposed TAML(Br)$_2$ during hydrolysis.

Oxidation of 1 in the Presence of Chloride Anions

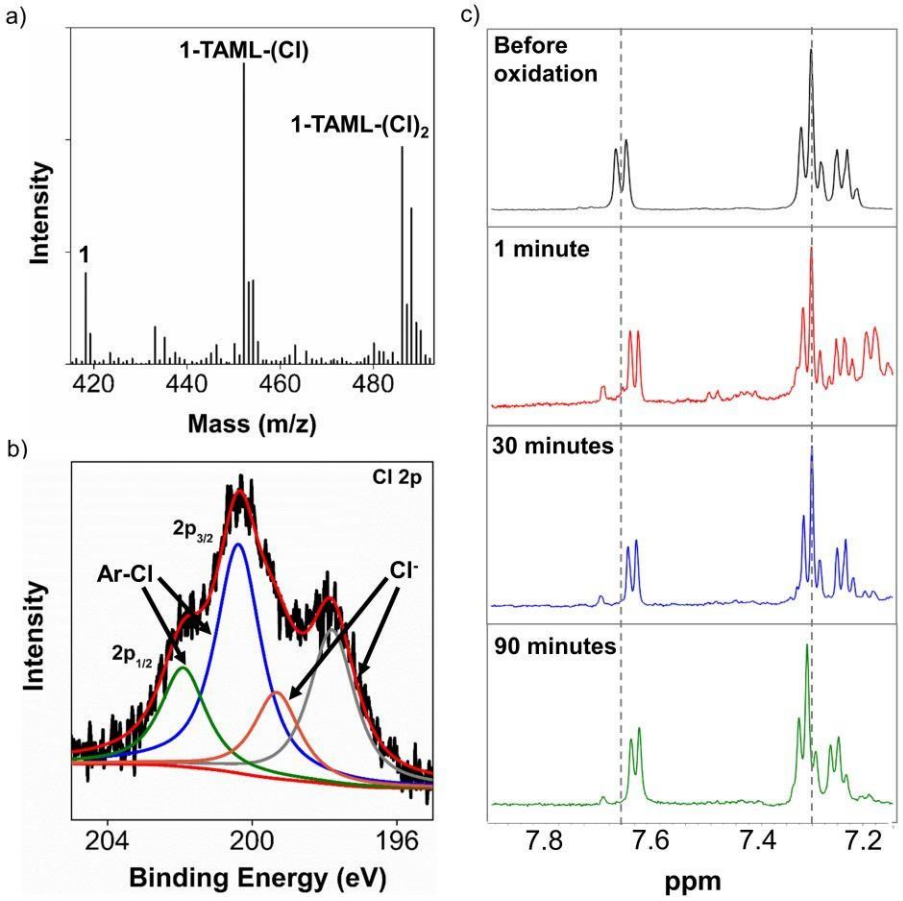

Fig. S16. (a) Negative-ion ESI-MS of the crude reaction mixture containing **1** (1 eq), $(ArMe)_3N\bullet^+$ (4 eq), and TEACl (10 eq) 18 hours after addition of the $(ArMe)_3N\bullet$+ oxidant. The assigned intermediates are shown. (b) Cl 2p XPS data. The fit (red) contains higher energy components (blue and green) assignable to aryl chloride, and lower energy components (grey and orange), corresponding to inorganic chloride ions. (c) ^{1}H NMR spectra of the deligated aliquots of reaction mixture **1** (1 eq) + $(ArMe)_3N\bullet^+$ (4 eq) + TEACl (10 eq), withdrawn at time intervals 1 (red), 30 (blue), and 90 (green) minutes after addition of the $(ArMe)_3N\bullet^+$ oxidant. The spectrum of TAML before oxidation is shown in black. The dashed lines highlight the characteristic ^{1}H NMR signals from TAML (grey). Due to the moderate conversions of TAML to TAML(Cl) and TAML$(Cl)_2$, based on the ESI-MS data, the ^{1}H NMR signals at different time points suggest slow reaction of the TAML, with small amounts of isomeric mixtures of TAML(Cl) and TAML$(Cl)_2$ as minor products.

Experiments to Probe the Mechanism for the Formation of 1(X)-TAML(X)$_n$

To probe if there is any interaction between **1** and X^- (X = Cl or Br), the UV-visible spectra of a solution of **1** (0.2 mM in ACN) before (black, **Fig. S17a**) and after the addition 10 equivalents of Cl^- (blue, **Fig. S17a**) or 10 equivalents of Br^- (red, **Fig. S17a**) were recorded. No further changes were noted upon further UV-visible spectroscopic measurements. We propose that these changes arise from the exchange of the solvent molecule at the axial position with a halide, thus forming **1(X)**, and this exchange reaches equilibrium within 3 minutes. In contrast, when CN^- was employed (*vide infra*) in place of halide anions, the UV-visible spectra of the mixture of **1** and 10 equivalents of CN^- reveal a more gradual equilibrium being achieved over 30 minutes (**Fig. S17b**). Compared to the spectra of **1(X)** (X = halide), a more distinct change in λ_{max} from 415 nm (red, **Fig. S17b**) to 440 nm (green, **Fig. S17b**) is observed. The small anodic shift in the first redox waves of **1** on going from Br^- to Cl^- to CN^- (increasing electron deficiency) also substantiate the exchange of solvent molecule at the axial position of **1** with the exogenous anions (**Fig. S17c**). In addition, the ESI-MS data show the presence of a mass fragment corresponding to K[**1**$^+$**(CN)$_2$**] upon the oxidation of **1** in the presence of excess CN^- (Main Text, **Fig. 8a**). These results suggest that, in the presence of excess CN^-, two CN^- ligands can exchange with the axial solvent molecules of **1** to form **1(CN)$_2$**.

Several experiments were performed to probe the possible mechanism of the formation of **1(X)-TAML(X)$_n$**. One of them is the reaction between 1,4-dimethoxybenzene (DMOB) and oxidised **1(Br)**. Through ^{1}H NMR spectroscopic studies and GC-MS analysis of the reaction mixture, no evidence of brominated DMOB (**Fig. S17e**) is observed. Using 1,1,2,2-tetrachloroethane as the internal standard, the amount of DMOB throughout the reaction was monitored. Due to the broadening and overlap with $(ArMe)_3N$ of the ^{1}H NMR signals, quantifying DMOB using the integration of the ^{1}H NMR signals is not as accurate as using GC-MS. We quantified the concentrations of DMOB using GC-MS with reference to an internal standard, and confirmed that the amount of DMOB remained unchanged throughout the reaction. Similar to the ESI-MS results of the reaction without DMOB, only bromide substitution on the TAML ligand is observed **(Fig. S17f).**

Another experiment involved the addition of 10 equivalents of Br^- to a solution of oxidised **1(Cl)** (generated in situ by adding 2 equivalents of $(ArMe)_3N^{\bullet+}$ to a solution of 1 equivalent of Cl^- and **1**). Before the addition of Br^-, and after 5 minutes of stirring the oxidised **1(Cl)** solution, the ESI-MS data of the reaction mixture did not show observable amounts of **1-TAML(Cl)**. Upon addition of Br^-, the black solution slowly turned reddish-brown over 2 hours. ESI-MS measurement of the resulting reaction mixture revealed predominantly **1-TAML(Br)$_n$** products being formed instead of the **1-TAML(Cl)$_n$** products expected for an intramolecular chloride migration (**Fig. S17g**).

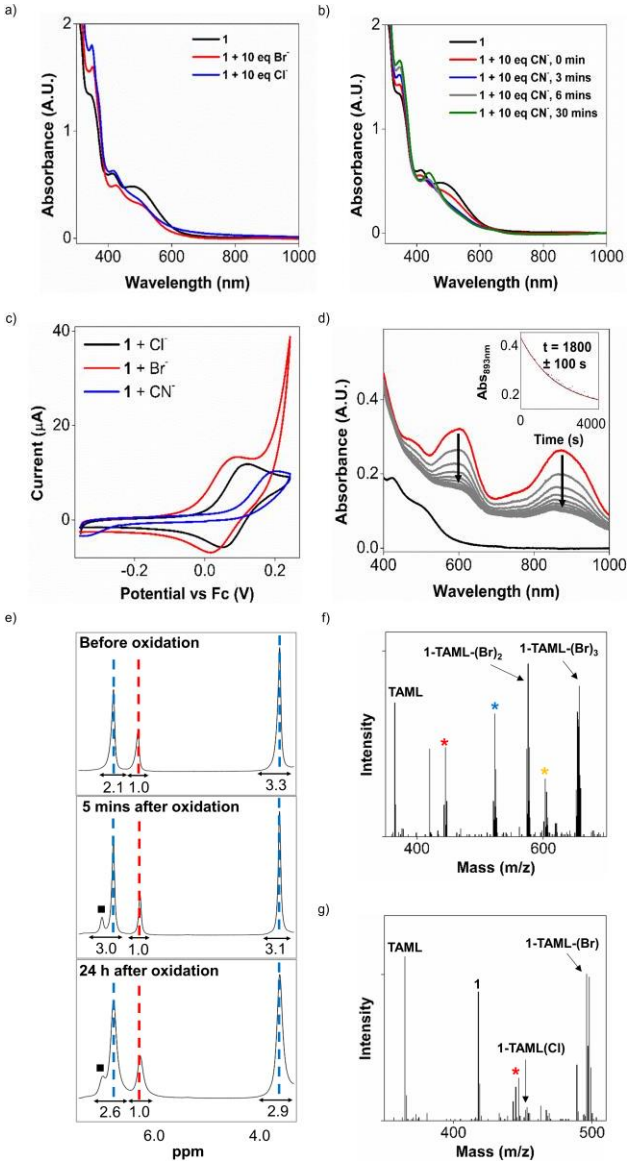

Fig. S17. (a) UV-vis spectrum of **1** (0.20 mM, black). UV-vis spectra of reaction mixtures of Br^- (10 eq) + **1** (red), and Cl^- (10 eq) + **1** (blue). The spectra of **1** in the presence of excess halide were measured at intervals of 3 minutes, and no further spectral changes were observed beyond 3 minutes. (b) UV-vis spectrum of **1** (0.20 mM, black) and the UV-vis spectral changes over time after the addition of CN^- (10 eq). (c) CV of **1** in the presence of 10 equivalents of Br^- (red), Cl^- (black), and CN^- (red). (d) UV-visible spectral changes from the reaction between oxidised **1(Br)** (0.20 mM) and TEABr (2.0 mM) in ACN. The inset shows the absorbance decay monitored at 893 nm (a characteristic band of the oxidised **1(Br)**), and the solid red line shows the fit to the kinetics. (e) ^1H NMR spectra of reaction mixture containing DMOB (10 eq), **1** (1 eq), TEABr (10 eq), and 1,1,2,2-tetrachloroethane as an internal standard, before (top), 5 minutes after (middle), and 24 hours after (bottom) the addition of $(ArMe)_3N\bullet^+$ (2 eq). The characteristic ^1H NMR signals from 1,1,2,2-tetrachloroethane (red dashed line), DMOB (blue dashed lines), and $(ArMe)_3N$ (■) are labelled. The areas under ^1H NMR signals are labelled in black. (f) Negative-ion ESI-MS of the reaction mixture of **1** (1 eq) + DMOB (10 eq) + Br^- (10 eq) + $(ArMe)_3N\bullet^+$ oxidant (2 eq). The assigned intermediates are labelled. The signals marked with * are assigned to TAML(Br) (red), TAML$(Br)_2$ (blue), and [TAML$(Br)_3$ (orange). (g) Negative-ion ESI-MS of the reaction mixture of **1** (1 eq) + Cl^- (1 eq) + $(ArMe)_3N\bullet^+$ oxidant (2 eq) after the addition of Br^- (10 eq). The signal marked with a red * is assigned to the deligated **1-TAML(Br)**.

Optimisation of the Oxidation of 1 in the Presence of Cyanide as a Nucleophile

Preliminary tests using the same experimental procedures as those used for Br^- as a nucleophile were conducted, with TEABr being replaced by potassium cyanide (KCN). Despite prolonged stirring (24 hours), no signal of **1-TAML(CN)$_n$** was observed by negative-ion mode ESI-MS. Furthermore, the black solution observed upon addition of $(ArMe)_3N\bullet^+$ remained black, unlike the Br^- and Cl^- experiments, where red suspensions were observed. We hypothesised that CN^- might have a stabilising effect on **1**$^+$, instead of undergoing nucleophilic substitution with **1-TAML**$\bullet^+$ to give **1-TAML(CN)$_n$**. We subsequently characterised the proposed CN^--stabilised **1**$^+$ species. The reaction mixture of **1**, ^{t}BuOK (1.1 equivalent), and KCN (5 equivalents) turned from red to black immediately upon addition of $(ArMe)_3N\bullet^+$ (1.05 equivalents). UV-vis spectroscopic measurement of the crude reaction mixture showed three characteristic peaks at 600, 677, and 837 nm, with an estimated lifetime, τ_{837nm}, of 4.4 ± 0.7 hours at room temperature (**Fig. S18a and S18b**). We also characterised the reaction mixture using infrared (IR) spectroscopy (**Fig. S18c**). The discussion on the C≡N vibrations can be found in the main text (**Figure 8b**).

Having determined that the CN^--stabilised **1**$^+$ was not stable in solution at room temperature, we modified the procedures. The product, **1**$^+$**(CN)$_2$** was characterised by X-ray crystallography (**Fig. S19**). Disorder was found in the TAML ligand, but not in the Fe-$(CN)_2$ core, and the data was refined to give two models, as shown in **Fig. S19a.** The crystallographic data are summarised in **Tables S2-6**.

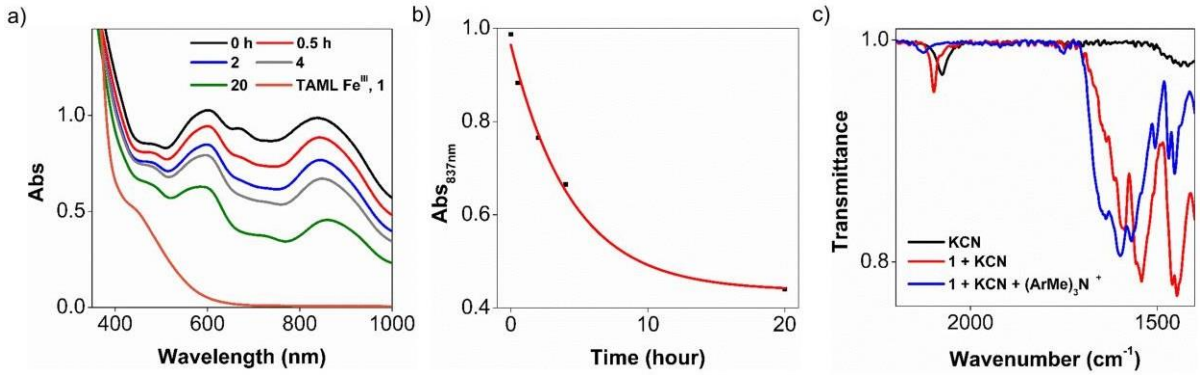

Fig. S18. (a) UV-vis spectrum of **1** (orange) and the UV-vis spectral changes over time upon oxidation of **1** by $(ArMe)_3N\bullet^+$ (1.05 eq) in the presence of excess of CN^- (5 eq.). (b) The change in absorbance, monitored at 837 nm over time. The mono-exponential fit is the line in red, giving an estimated lifetime, τ_{837nm}, of 4.4 ± 0.7 hours. (c) Infrared spectra of KCN (black, υ_{CN}(KCN) = 2076 cm^{-1}); **1** (1 eq) + ^{t}BuOK (1.1 eq) + KCN (5 eq) (red, υ_{CN}[Fe^{III}(CN)] = 2098 cm^{-1}); and **1** (1 eq) + ^{t}BuOK (1.1 eq) + KCN (5 eq) + $(ArMe)_3N\bullet^+$ (1.05 eq) (blue, υ_{CN} [Fe^{IV}(CN)] = 2127 cm^{-1}).

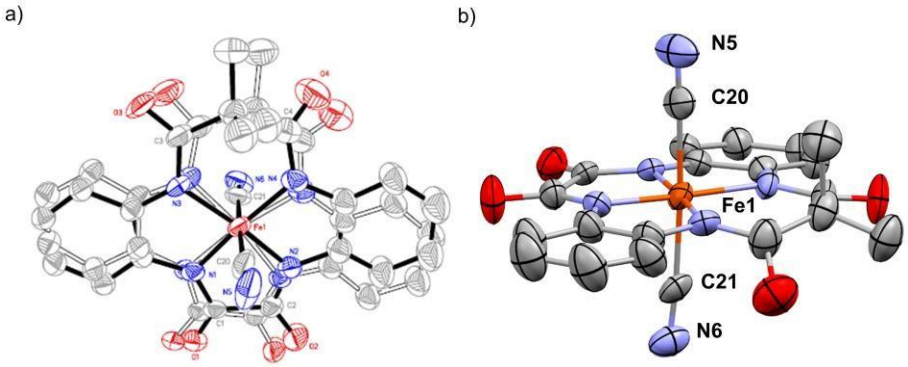

Fig. S19. (a) ORTEP image of the X-ray crystal structure of complex $(PPh_4)_2[\mathbf{1^+(CN)_2}]$, with disorder in the TAML ligand. The disorder has been refined to two models over two positions (grey and black solid lines). The hydrogen atoms and PPh_4^+ cations have been omitted for clarity. The ellipsoids are drawn at 50% probability. Selected bond lengths (Å): Fe1-C20 2.011(6), Fe1-C21 1.993(6), C20-N5 1.137(7), C21-N6 1.141(7). (b) ORTEP image of the X-ray crystal structure of complex $(PPh_4)_2[\mathbf{1^+(CN)_2}]$. Atom colours: grey for carbon, blue for nitrogen, red for oxygen, and orange for iron.

Table S2. Crystal data and structure refinement for $\mathbf{1^+(CN)_2}$.

Identification code	$\mathbf{1^+(CN)_2}$	
Empirical formula	C69 H54 Fe N6 O4 P2	
Formula weight	1148.97	
Temperature	160(2) K	
Wavelength	1.54178 Å	
Crystal system	Monoclinic	
Space group	$P2_1/c$	
Unit cell dimensions	a = 17.9956(3) Å	α = 90°.
	b = 14.2843(2) Å	β = 111.3696(10)°.
	c = 23.6299(3) Å	γ = 90°.
Volume	5656.57(15) $Å^3$	
Z	4	
Density (calculated)	1.349 Mg/m^3	
Absorption coefficient	3.129 mm^{-1}	
F(000)	2392	
Crystal size	0.200 x 0.160 x 0.140 mm^3	
Theta range for data collection	2.637 to 66.672°.	
Index ranges	-21<=h<=20, -16<=k<=16, -27<=l<=28	
Reflections collected	34162	
Independent reflections	9856 [R(int) = 0.0514]	
Completeness to theta = 66.672°	98.5 %	
Absorption correction	None	
Refinement method	Full-matrix least-squares on F^2	
Data / restraints / parameters	9856 / 1752 / 969	

Goodness-of-fit on F^2	1.065
Final R indices [I>2sigma(I)]	R1 = 0.0852, wR2 = 0.2194
R indices (all data)	R1 = 0.1020, wR2 = 0.2320
Extinction coefficient	n/a
Largest diff. peak and hole	1.640 and -0.489 e.Å^{-3}

Table S3. Atomic coordinates (x 10^4) and equivalent isotropic displacement parameters (Å^{2}x 10^3) for **$1^+(CN)_2$**. U(eq) is defined as one third of the trace of the orthogonalized U^{ij} tensor.

	x	y	z	U(eq)
Fe(1)	7588(1)	7369(1)	1337(1)	38(1)
C(1)	7005(6)	5723(7)	1459(5)	36(2)
C(2)	7873(7)	5738(8)	1897(5)	41(2)
C(3)	6988(7)	8991(6)	541(4)	43(2)
C(4)	8528(7)	8960(9)	1282(6)	61(2)
C(5)	7770(8)	9473(7)	899(4)	54(2)
C(6)	7595(8)	9937(10)	1435(5)	66(2)
C(7)	7948(9)	10286(9)	581(6)	76(3)
C(8)	6084(8)	6753(9)	658(7)	38(2)
C(9)	5421(7)	6179(8)	419(6)	43(2)
C(10)	4778(6)	6487(8)	-89(5)	47(2)
C(11)	4792(6)	7364(9)	-328(5)	44(2)
C(12)	5436(6)	7969(8)	-77(5)	41(2)
C(13)	6097(6)	7657(9)	418(6)	38(2)
C(14)	9004(6)	6861(8)	2199(5)	49(2)
C(15)	9610(6)	6341(8)	2614(6)	67(2)
C(16)	10340(7)	6748(10)	2924(7)	77(3)
C(17)	10491(7)	7645(9)	2747(7)	80(3)
C(18)	9913(6)	8160(8)	2313(6)	64(2)
C(19)	9166(5)	7763(7)	2027(5)	49(2)
O(1)	6601(6)	5009(7)	1389(5)	50(2)
O(2)	8174(6)	5045(6)	2210(5)	65(2)
O(3)	6560(6)	9435(6)	102(4)	66(2)
O(4)	9141(6)	9084(8)	1119(5)	84(2)
N(1)	6774(7)	6542(9)	1159(7)	35(2)
N(2)	8227(5)	6572(7)	1897(5)	39(2)
N(3)	6820(6)	8150(8)	721(6)	36(2)

N(4)	8495(5)	8184(6)	1583(4)	42(2)
C(1A)	6762(7)	5658(8)	1327(6)	35(2)
C(2A)	7600(7)	5533(8)	1799(6)	36(2)
C(3A)	7334(8)	8863(8)	511(5)	47(2)
C(5A)	8790(8)	8491(10)	1287(6)	56(2)
C(4A)	8160(8)	9220(8)	910(5)	49(2)
C(6A)	8033(10)	9762(11)	1427(6)	66(2)
C(7A)	8485(11)	9809(11)	559(7)	76(3)
C(8A)	6065(9)	6882(11)	578(8)	38(2)
C(9A)	5347(8)	6405(10)	270(6)	43(2)
C(10A)	4779(7)	6831(11)	-228(6)	45(2)
C(11A)	4938(8)	7702(10)	-413(6)	45(2)
C(12A)	5659(7)	8169(9)	-119(6)	41(2)
C(13A)	6246(8)	7755(10)	374(7)	38(2)
C(14A)	8869(3)	6433(6)	2171(4)	43(2)
C(15A)	9371(4)	5834(5)	2607(4)	52(2)
C(16A)	10160(4)	6087(6)	2925(4)	62(2)
C(17A)	10447(4)	6939(7)	2806(4)	64(3)
C(18A)	9945(5)	7538(6)	2370(4)	57(2)
C(19A)	9156(4)	7286(6)	2053(4)	46(2)
O(1A)	6277(6)	5019(8)	1223(5)	42(2)
O(2A)	7809(6)	4802(6)	2095(4)	50(2)
O(3A)	7049(8)	9156(8)	-8(4)	80(3)
O(4A)	9508(7)	8499(10)	1286(6)	89(3)
N(1A)	6689(9)	6517(10)	1067(9)	36(2)
N(2A)	8076(6)	6293(8)	1840(5)	35(2)
N(3A)	7012(7)	8135(9)	708(7)	37(2)
N(4A)	8607(5)	7876(8)	1625(5)	45(2)
C(20)	7275(3)	7944(4)	1995(2)	49(1)
C(21)	7931(3)	6745(4)	719(2)	45(1)
N(5)	7123(3)	8256(5)	2382(2)	70(2)
N(6)	8144(3)	6344(4)	388(2)	55(1)
C(22)	6007(3)	511(3)	3433(2)	37(1)
C(23)	6044(4)	-347(4)	3159(3)	49(1)
C(24)	6295(4)	-1137(4)	3507(3)	54(1)
C(25)	6507(3)	-1082(4)	4131(3)	50(1)
C(26)	6475(3)	-232(4)	4403(3)	48(1)
C(27)	6222(3)	562(4)	4057(2)	41(1)

C(28)	6341(3)	1847(4)	2598(2)	43(1)
C(29)	6967(4)	1290(5)	2628(3)	70(2)
C(30)	7501(5)	1608(6)	2363(4)	99(3)
C(31)	7372(5)	2427(6)	2056(4)	99(3)
C(32)	6769(4)	2995(5)	2038(3)	67(2)
C(33)	6252(3)	2719(4)	2321(2)	45(1)
C(34)	5554(3)	2505(3)	3386(2)	36(1)
C(35)	4808(3)	2819(3)	3355(2)	38(1)
C(36)	4751(3)	3588(4)	3698(3)	48(1)
C(37)	5432(4)	4042(4)	4061(3)	53(1)
C(38)	6169(4)	3741(4)	4090(3)	55(2)
C(39)	6237(3)	2977(4)	3754(3)	49(1)
C(40)	4704(3)	1193(3)	2387(2)	35(1)
C(41)	4165(3)	697(3)	2572(3)	45(1)
C(42)	3444(3)	441(4)	2147(3)	54(1)
C(43)	3253(4)	669(4)	1547(3)	55(2)
C(44)	3774(3)	1171(4)	1364(3)	52(1)
C(45)	4506(3)	1442(3)	1783(2)	41(1)
C(46)	1003(3)	8132(3)	663(3)	40(1)
C(47)	1364(3)	8104(4)	1287(3)	51(1)
C(48)	1520(4)	8920(4)	1623(3)	61(2)
C(49)	1325(3)	9761(4)	1328(4)	63(2)
C(50)	985(3)	9801(4)	711(4)	63(2)
C(51)	815(3)	8997(3)	369(3)	48(1)
C(52)	-223(3)	7271(3)	-364(2)	43(1)
C(53)	-352(4)	7263(5)	-974(3)	71(2)
C(54)	-1093(5)	7472(5)	-1405(3)	79(2)
C(55)	-1722(4)	7649(4)	-1241(3)	57(2)
C(56)	-1621(4)	7728(5)	-639(3)	66(2)
C(57)	-872(4)	7541(5)	-202(3)	67(2)
C(58)	1436(3)	6830(3)	-152(3)	45(1)
C(59)	2035(4)	7449(4)	-114(3)	56(2)
C(60)	2553(4)	7247(5)	-410(3)	66(2)
C(61)	2471(4)	6449(4)	-738(3)	59(2)
C(62)	1876(5)	5838(4)	-775(4)	83(2)
C(63)	1374(5)	6014(4)	-459(4)	82(2)
C(64)	762(3)	6140(3)	729(2)	40(1)
C(65)	205(5)	6099(5)	998(4)	85(3)

C(66)	285(5)	5475(5)	1456(4)	79(2)
C(67)	919(4)	4875(4)	1651(3)	56(2)
C(68)	1471(4)	4890(5)	1381(4)	80(2)
C(69)	1404(4)	5523(4)	928(4)	67(2)
P(1)	5652(1)	1513(1)	2954(1)	33(1)
P(2)	737(1)	7078(1)	214(1)	38(1)

Table S4. Bond lengths [Å] and angles [°] for $\mathbf{1^{+}(CN)_2}$.

Fe(1)-N(2)	1.807(9)
Fe(1)-N(1)	1.807(11)
Fe(1)-N(3A)	1.832(11)
Fe(1)-N(4A)	1.856(9)
Fe(1)-N(4)	1.916(8)
Fe(1)-N(1A)	1.938(12)
Fe(1)-N(2A)	1.946(10)
Fe(1)-N(3)	1.950(9)
Fe(1)-C(21)	1.993(6)
Fe(1)-C(20)	2.011(6)
C(1)-O(1)	1.227(11)
C(1)-N(1)	1.353(10)
C(1)-C(2)	1.528(13)
C(2)-O(2)	1.236(10)
C(2)-N(2)	1.350(12)
C(3)-O(3)	1.219(10)
C(3)-N(3)	1.346(11)
C(3)-C(5)	1.517(13)
C(4)-O(4)	1.306(13)
C(4)-N(4)	1.329(13)
C(4)-C(5)	1.522(16)
C(5)-C(7)	1.480(13)
C(5)-C(6)	1.561(15)
C(8)-C(9)	1.388(11)
C(8)-N(1)	1.400(10)
C(8)-C(13)	1.414(11)
C(9)-C(10)	1.399(13)
C(10)-C(11)	1.378(14)

C(11)-C(12)	1.392(14)
C(12)-C(13)	1.403(11)
C(13)-N(3)	1.422(11)
C(14)-N(2)	1.382(11)
C(14)-C(15)	1.387(12)
C(14)-C(19)	1.414(12)
C(15)-C(16)	1.377(13)
C(16)-C(17)	1.405(14)
C(17)-C(18)	1.378(13)
C(18)-C(19)	1.386(12)
C(19)-N(4)	1.413(11)
C(1A)-O(1A)	1.225(12)
C(1A)-N(1A)	1.357(12)
C(1A)-C(2A)	1.525(14)
C(2A)-O(2A)	1.237(11)
C(2A)-N(2A)	1.364(13)
C(3A)-O(3A)	1.219(12)
C(3A)-N(3A)	1.353(12)
C(3A)-C(4A)	1.528(15)
C(5A)-O(4A)	1.294(14)
C(5A)-N(4A)	1.308(14)
C(5A)-C(4A)	1.558(17)
C(4A)-C(7A)	1.445(14)
C(4A)-C(6A)	1.533(16)
C(8A)-N(1A)	1.387(11)
C(8A)-C(9A)	1.407(12)
C(8A)-C(13A)	1.417(13)
C(9A)-C(10A)	1.385(15)
C(10A)-C(11A)	1.382(16)
C(11A)-C(12A)	1.398(15)
C(12A)-C(13A)	1.387(12)
C(13A)-N(3A)	1.423(12)
C(14A)-N(2A)	1.370(10)
C(14A)-C(15A)	1.3900
C(14A)-C(19A)	1.3900
C(15A)-C(16A)	1.3900
C(16A)-C(17A)	1.3900
C(17A)-C(18A)	1.3900

C(18A)-C(19A)	1.3900
C(19A)-N(4A)	1.407(11)
C(20)-N(5)	1.137(7)
C(21)-N(6)	1.141(7)
C(22)-C(27)	1.384(7)
C(22)-C(23)	1.399(7)
C(22)-P(1)	1.792(5)
C(23)-C(24)	1.373(7)
C(24)-C(25)	1.384(8)
C(25)-C(26)	1.385(8)
C(26)-C(27)	1.376(7)
C(28)-C(29)	1.360(8)
C(28)-C(33)	1.389(7)
C(28)-P(1)	1.798(5)
C(29)-C(30)	1.403(9)
C(30)-C(31)	1.351(10)
C(31)-C(32)	1.343(10)
C(32)-C(33)	1.385(8)
C(34)-C(35)	1.393(7)
C(34)-C(39)	1.394(7)
C(34)-P(1)	1.791(5)
C(35)-C(36)	1.391(7)
C(36)-C(37)	1.375(8)
C(37)-C(38)	1.372(9)
C(38)-C(39)	1.380(8)
C(40)-C(45)	1.386(7)
C(40)-C(41)	1.393(7)
C(40)-P(1)	1.802(5)
C(41)-C(42)	1.370(8)
C(42)-C(43)	1.371(9)
C(43)-C(44)	1.370(8)
C(44)-C(45)	1.384(8)
C(46)-C(47)	1.380(8)
C(46)-C(51)	1.397(7)
C(46)-P(2)	1.802(5)
C(47)-C(48)	1.380(8)
C(48)-C(49)	1.368(9)
C(49)-C(50)	1.360(10)

C(50)-C(51)	1.375(8)
C(52)-C(53)	1.375(9)
C(52)-C(57)	1.410(9)
C(52)-P(2)	1.790(6)
C(53)-C(54)	1.384(10)
C(54)-C(55)	1.349(10)
C(55)-C(56)	1.370(9)
C(56)-C(57)	1.393(9)
C(58)-C(63)	1.356(8)
C(58)-C(59)	1.371(7)
C(58)-P(2)	1.805(5)
C(59)-C(60)	1.385(8)
C(60)-C(61)	1.356(9)
C(61)-C(62)	1.359(10)
C(62)-C(63)	1.390(9)
C(64)-C(65)	1.370(8)
C(64)-C(69)	1.392(8)
C(64)-P(2)	1.798(5)
C(65)-C(66)	1.367(9)
C(66)-C(67)	1.366(9)
C(67)-C(68)	1.362(10)
C(68)-C(69)	1.373(9)

N(2)-Fe(1)-N(1)	90.2(4)
N(3A)-Fe(1)-N(4A)	104.9(4)
N(2)-Fe(1)-N(4)	85.2(4)
N(1)-Fe(1)-N(4)	175.3(4)
N(3A)-Fe(1)-N(1A)	87.1(4)
N(4A)-Fe(1)-N(1A)	164.0(7)
N(3A)-Fe(1)-N(2A)	164.4(6)
N(4A)-Fe(1)-N(2A)	85.3(4)
N(1A)-Fe(1)-N(2A)	80.9(4)
N(2)-Fe(1)-N(3)	174.8(4)
N(1)-Fe(1)-N(3)	84.6(4)
N(4)-Fe(1)-N(3)	100.0(4)
N(2)-Fe(1)-C(21)	88.3(4)
N(1)-Fe(1)-C(21)	88.7(7)
N(3A)-Fe(1)-C(21)	84.7(6)

N(4A)-Fe(1)-C(21)	85.1(4)
N(4)-Fe(1)-C(21)	92.1(4)
N(1A)-Fe(1)-C(21)	85.5(8)
N(2A)-Fe(1)-C(21)	84.4(4)
N(3)-Fe(1)-C(21)	91.9(5)
N(2)-Fe(1)-C(20)	88.5(4)
N(1)-Fe(1)-C(20)	90.9(7)
N(3A)-Fe(1)-C(20)	98.6(6)
N(4A)-Fe(1)-C(20)	94.3(5)
N(4)-Fe(1)-C(20)	88.0(4)
N(1A)-Fe(1)-C(20)	94.4(8)
N(2A)-Fe(1)-C(20)	92.4(4)
N(3)-Fe(1)-C(20)	91.3(5)
C(21)-Fe(1)-C(20)	176.7(2)
O(1)-C(1)-N(1)	126.5(10)
O(1)-C(1)-C(2)	120.8(9)
N(1)-C(1)-C(2)	112.6(8)
O(2)-C(2)-N(2)	127.0(10)
O(2)-C(2)-C(1)	120.7(10)
N(2)-C(2)-C(1)	112.3(7)
O(3)-C(3)-N(3)	126.0(10)
O(3)-C(3)-C(5)	114.1(8)
N(3)-C(3)-C(5)	119.9(8)
O(4)-C(4)-N(4)	118.5(12)
O(4)-C(4)-C(5)	115.4(10)
N(4)-C(4)-C(5)	121.0(9)
C(7)-C(5)-C(3)	113.7(9)
C(7)-C(5)-C(4)	111.5(11)
C(3)-C(5)-C(4)	124.1(9)
C(7)-C(5)-C(6)	102.9(10)
C(3)-C(5)-C(6)	103.0(10)
C(4)-C(5)-C(6)	97.1(9)
C(9)-C(8)-N(1)	125.7(9)
C(9)-C(8)-C(13)	120.8(9)
N(1)-C(8)-C(13)	113.4(9)
C(8)-C(9)-C(10)	118.9(10)
C(11)-C(10)-C(9)	120.2(9)
C(10)-C(11)-C(12)	121.8(9)

C(11)-C(12)-C(13)	118.6(10)
C(12)-C(13)-C(8)	119.5(9)
C(12)-C(13)-N(3)	127.3(9)
C(8)-C(13)-N(3)	113.3(8)
N(2)-C(14)-C(15)	126.3(10)
N(2)-C(14)-C(19)	113.6(8)
C(15)-C(14)-C(19)	120.0(9)
C(16)-C(15)-C(14)	120.2(11)
C(15)-C(16)-C(17)	118.5(11)
C(18)-C(17)-C(16)	122.2(11)
C(17)-C(18)-C(19)	118.6(10)
C(18)-C(19)-N(4)	127.0(9)
C(18)-C(19)-C(14)	119.8(9)
N(4)-C(19)-C(14)	113.1(8)
C(1)-N(1)-C(8)	129.5(10)
C(1)-N(1)-Fe(1)	112.1(7)
C(8)-N(1)-Fe(1)	116.7(7)
C(2)-N(2)-C(14)	130.7(9)
C(2)-N(2)-Fe(1)	112.4(6)
C(14)-N(2)-Fe(1)	116.4(7)
C(3)-N(3)-C(13)	123.5(8)
C(3)-N(3)-Fe(1)	124.5(7)
C(13)-N(3)-Fe(1)	111.2(6)
C(4)-N(4)-C(19)	124.0(8)
C(4)-N(4)-Fe(1)	122.9(7)
C(19)-N(4)-Fe(1)	111.7(6)
O(1A)-C(1A)-N(1A)	129.7(11)
O(1A)-C(1A)-C(2A)	120.1(10)
N(1A)-C(1A)-C(2A)	110.1(9)
O(2A)-C(2A)-N(2A)	125.4(11)
O(2A)-C(2A)-C(1A)	121.9(11)
N(2A)-C(2A)-C(1A)	112.7(8)
O(3A)-C(3A)-N(3A)	122.3(11)
O(3A)-C(3A)-C(4A)	117.6(10)
N(3A)-C(3A)-C(4A)	119.2(9)
O(4A)-C(5A)-N(4A)	118.7(13)
O(4A)-C(5A)-C(4A)	120.8(11)
N(4A)-C(5A)-C(4A)	120.4(11)

C(7A)-C(4A)-C(3A)	110.3(10)
C(7A)-C(4A)-C(6A)	111.8(11)
C(3A)-C(4A)-C(6A)	105.3(12)
C(7A)-C(4A)-C(5A)	110.8(12)
C(3A)-C(4A)-C(5A)	118.1(9)
C(6A)-C(4A)-C(5A)	99.8(10)
N(1A)-C(8A)-C(9A)	124.2(11)
N(1A)-C(8A)-C(13A)	113.4(10)
C(9A)-C(8A)-C(13A)	122.1(10)
C(10A)-C(9A)-C(8A)	118.8(12)
C(11A)-C(10A)-C(9A)	119.3(11)
C(10A)-C(11A)-C(12A)	122.2(11)
C(13A)-C(12A)-C(11A)	119.9(11)
C(12A)-C(13A)-C(8A)	117.5(10)
C(12A)-C(13A)-N(3A)	126.2(10)
C(8A)-C(13A)-N(3A)	116.3(9)
N(2A)-C(14A)-C(15A)	126.5(7)
N(2A)-C(14A)-C(19A)	113.5(7)
C(15A)-C(14A)-C(19A)	120.0
C(16A)-C(15A)-C(14A)	120.0
C(15A)-C(16A)-C(17A)	120.0
C(18A)-C(17A)-C(16A)	120.0
C(19A)-C(18A)-C(17A)	120.0
C(18A)-C(19A)-C(14A)	120.0
C(18A)-C(19A)-N(4A)	122.9(6)
C(14A)-C(19A)-N(4A)	117.0(6)
C(1A)-N(1A)-C(8A)	129.3(11)
C(1A)-N(1A)-Fe(1)	119.2(8)
C(8A)-N(1A)-Fe(1)	111.3(8)
C(2A)-N(2A)-C(14A)	130.8(9)
C(2A)-N(2A)-Fe(1)	117.0(7)
C(14A)-N(2A)-Fe(1)	112.2(7)
C(3A)-N(3A)-C(13A)	123.5(10)
C(3A)-N(3A)-Fe(1)	123.4(8)
C(13A)-N(3A)-Fe(1)	111.7(7)
C(5A)-N(4A)-C(19A)	125.1(10)
C(5A)-N(4A)-Fe(1)	118.2(9)
C(19A)-N(4A)-Fe(1)	111.8(7)

N(5)-C(20)-Fe(1)	177.5(5)
N(6)-C(21)-Fe(1)	175.9(5)
C(27)-C(22)-C(23)	119.8(5)
C(27)-C(22)-P(1)	121.9(4)
C(23)-C(22)-P(1)	118.3(4)
C(24)-C(23)-C(22)	120.2(5)
C(23)-C(24)-C(25)	119.6(5)
C(24)-C(25)-C(26)	120.2(5)
C(27)-C(26)-C(25)	120.5(5)
C(26)-C(27)-C(22)	119.6(5)
C(29)-C(28)-C(33)	120.0(5)
C(29)-C(28)-P(1)	121.3(4)
C(33)-C(28)-P(1)	118.6(4)
C(28)-C(29)-C(30)	118.5(6)
C(31)-C(30)-C(29)	120.5(6)
C(32)-C(31)-C(30)	121.3(6)
C(31)-C(32)-C(33)	119.3(6)
C(32)-C(33)-C(28)	120.1(6)
C(35)-C(34)-C(39)	119.3(5)
C(35)-C(34)-P(1)	121.2(4)
C(39)-C(34)-P(1)	119.5(4)
C(36)-C(35)-C(34)	119.9(5)
C(37)-C(36)-C(35)	119.9(5)
C(38)-C(37)-C(36)	120.6(5)
C(37)-C(38)-C(39)	120.3(5)
C(38)-C(39)-C(34)	120.0(5)
C(45)-C(40)-C(41)	120.4(5)
C(45)-C(40)-P(1)	121.2(4)
C(41)-C(40)-P(1)	118.3(4)
C(42)-C(41)-C(40)	119.2(5)
C(41)-C(42)-C(43)	120.5(5)
C(44)-C(43)-C(42)	120.5(5)
C(43)-C(44)-C(45)	120.2(5)
C(44)-C(45)-C(40)	119.1(5)
C(47)-C(46)-C(51)	119.5(5)
C(47)-C(46)-P(2)	121.7(4)
C(51)-C(46)-P(2)	118.8(4)
C(46)-C(47)-C(48)	120.5(6)

C(49)-C(48)-C(47)	119.3(6)
C(50)-C(49)-C(48)	120.9(5)
C(49)-C(50)-C(51)	120.8(6)
C(50)-C(51)-C(46)	119.0(6)
C(53)-C(52)-C(57)	116.6(6)
C(53)-C(52)-P(2)	123.2(5)
C(57)-C(52)-P(2)	119.9(4)
C(52)-C(53)-C(54)	121.3(6)
C(55)-C(54)-C(53)	120.9(7)
C(54)-C(55)-C(56)	120.4(6)
C(55)-C(56)-C(57)	118.8(6)
C(56)-C(57)-C(52)	121.6(6)
C(63)-C(58)-C(59)	120.0(5)
C(63)-C(58)-P(2)	119.3(4)
C(59)-C(58)-P(2)	120.7(4)
C(58)-C(59)-C(60)	119.4(6)
C(61)-C(60)-C(59)	120.7(6)
C(60)-C(61)-C(62)	119.8(6)
C(61)-C(62)-C(63)	120.0(7)
C(58)-C(63)-C(62)	120.0(6)
C(65)-C(64)-C(69)	118.3(5)
C(65)-C(64)-P(2)	120.2(4)
C(69)-C(64)-P(2)	120.9(4)
C(66)-C(65)-C(64)	120.8(6)
C(67)-C(66)-C(65)	120.6(6)
C(68)-C(67)-C(66)	119.7(6)
C(67)-C(68)-C(69)	120.2(6)
C(68)-C(69)-C(64)	120.5(6)
C(34)-P(1)-C(22)	111.0(2)
C(34)-P(1)-C(28)	106.5(2)
C(22)-P(1)-C(28)	111.0(2)
C(34)-P(1)-C(40)	111.2(2)
C(22)-P(1)-C(40)	106.9(2)
C(28)-P(1)-C(40)	110.3(2)
C(52)-P(2)-C(64)	114.2(2)
C(52)-P(2)-C(46)	107.2(2)
C(64)-P(2)-C(46)	106.8(2)
C(52)-P(2)-C(58)	108.1(3)

C(64)-P(2)-C(58)	109.1(2)
C(46)-P(2)-C(58)	111.3(2)

Symmetry transformations used to generate equivalent atoms:

Table S5. Anisotropic displacement parameters ($Å^2 x\ 10^3$) for $\mathbf{1^+(CN)_2}$. The anisotropic displacement factor exponent takes the form: $-2\pi^2[h^2 a^{*2} U^{11} + ... + 2 h k a^* b^* U^{12}]$

	U^{11}	U^{22}	U^{33}	U^{23}	U^{13}	U^{12}
Fe(1)	38(1)	46(1)	30(1)	12(1)	14(1)	7(1)
C(1)	39(3)	39(3)	38(3)	9(3)	24(3)	5(3)
C(2)	38(3)	41(3)	45(3)	12(3)	16(3)	8(3)
C(3)	55(3)	39(3)	31(3)	9(2)	11(3)	-1(3)
C(4)	54(3)	55(4)	71(3)	14(3)	21(3)	-6(3)
C(5)	63(4)	46(3)	46(3)	4(3)	12(3)	-12(3)
C(6)	71(5)	63(4)	57(3)	-9(3)	15(4)	-9(4)
C(7)	80(6)	72(6)	75(6)	24(5)	27(5)	-15(5)
C(8)	39(3)	40(3)	39(3)	5(3)	19(3)	8(2)
C(9)	42(3)	43(4)	48(4)	6(3)	21(3)	5(3)
C(10)	43(3)	44(4)	52(4)	4(3)	16(3)	1(3)
C(11)	43(3)	40(4)	45(3)	3(3)	11(3)	-1(3)
C(12)	43(3)	39(4)	39(3)	4(3)	12(3)	-1(3)
C(13)	41(3)	40(3)	34(3)	0(2)	14(3)	2(3)
C(14)	38(3)	47(3)	61(3)	8(3)	17(2)	8(3)
C(15)	47(3)	58(3)	81(3)	9(3)	7(3)	8(3)
C(16)	48(3)	70(4)	95(4)	9(4)	4(3)	6(3)
C(17)	49(4)	73(4)	103(5)	7(4)	9(4)	8(3)
C(18)	41(3)	61(4)	87(4)	3(4)	19(3)	3(3)
C(19)	39(3)	49(3)	62(3)	6(3)	21(3)	4(3)
O(1)	49(5)	48(4)	57(5)	13(3)	23(4)	-3(4)
O(2)	54(5)	45(4)	80(5)	31(4)	4(4)	4(3)
O(3)	78(5)	51(4)	51(4)	31(3)	2(4)	5(4)
O(4)	74(4)	91(6)	97(5)	4(5)	43(4)	-18(4)
N(1)	37(3)	40(3)	36(4)	8(3)	23(3)	8(3)
N(2)	36(3)	40(3)	45(3)	8(3)	20(2)	8(2)
N(3)	46(4)	34(3)	26(3)	8(2)	10(3)	5(3)
N(4)	42(3)	48(4)	45(3)	3(3)	26(2)	1(3)

C(1A)	32(4)	40(3)	37(4)	7(3)	18(3)	2(3)
C(2A)	36(3)	37(3)	39(3)	8(3)	19(3)	1(3)
C(3A)	60(4)	45(3)	35(3)	8(3)	14(3)	-5(3)
C(5A)	59(3)	53(4)	58(3)	2(3)	23(3)	-11(3)
C(4A)	60(4)	43(3)	44(3)	-2(3)	20(3)	-11(3)
C(6A)	71(5)	63(4)	57(3)	-9(3)	15(4)	-9(4)
C(7A)	93(7)	72(6)	64(6)	14(5)	30(5)	-14(5)
C(8A)	39(3)	42(3)	37(3)	4(3)	18(3)	9(3)
C(9A)	42(3)	46(4)	44(4)	4(3)	18(3)	5(3)
C(10A)	42(3)	47(4)	46(4)	6(3)	15(3)	5(3)
C(11A)	46(4)	47(4)	43(4)	2(3)	15(3)	6(3)
C(12A)	44(4)	42(4)	36(3)	2(3)	15(3)	7(3)
C(13A)	43(3)	39(3)	33(3)	1(3)	16(3)	6(3)
C(14A)	34(3)	45(3)	53(3)	4(3)	20(3)	4(3)
C(15A)	36(3)	51(4)	66(4)	8(4)	16(3)	4(3)
C(16A)	41(4)	63(4)	75(4)	6(4)	13(3)	3(3)
C(17A)	39(4)	66(4)	83(4)	11(4)	19(3)	-1(3)
C(18A)	40(3)	59(3)	73(3)	5(3)	21(3)	-1(3)
C(19A)	37(3)	51(3)	57(3)	3(3)	24(2)	1(3)
O(1A)	39(5)	47(4)	42(5)	10(4)	16(4)	-10(4)
O(2A)	45(5)	39(4)	54(5)	14(3)	2(4)	-5(3)
O(3A)	105(7)	79(6)	41(4)	23(4)	7(4)	-17(5)
O(4A)	73(5)	98(7)	98(6)	18(6)	36(5)	-9(5)
N(1A)	36(3)	39(3)	37(4)	7(3)	20(3)	4(3)
N(2A)	31(3)	38(4)	40(3)	9(3)	18(3)	5(3)
N(3A)	45(4)	36(3)	28(3)	2(3)	13(3)	5(3)
N(4A)	43(3)	48(4)	50(3)	1(3)	25(3)	1(3)
C(20)	37(3)	70(4)	35(3)	10(3)	5(2)	15(3)
C(21)	50(3)	48(3)	44(3)	4(2)	27(3)	-13(2)
N(5)	48(3)	115(5)	39(3)	-2(3)	6(2)	30(3)
N(6)	61(3)	59(3)	55(3)	-10(2)	33(3)	-18(2)
C(22)	38(3)	33(2)	47(3)	7(2)	24(2)	1(2)
C(23)	66(4)	38(3)	55(3)	8(2)	38(3)	7(2)
C(24)	73(4)	31(3)	69(4)	9(3)	38(3)	9(3)
C(25)	54(3)	38(3)	62(4)	19(3)	24(3)	5(2)
C(26)	55(3)	43(3)	48(3)	6(2)	22(3)	-6(2)
C(27)	41(3)	37(3)	50(3)	4(2)	22(2)	-3(2)
C(28)	35(3)	46(3)	51(3)	16(2)	21(2)	1(2)

C(29)	64(4)	79(4)	86(5)	49(4)	50(4)	34(3)
C(30)	84(5)	121(7)	130(7)	82(6)	83(5)	56(5)
C(31)	67(5)	130(7)	127(7)	84(6)	68(5)	31(5)
C(32)	72(4)	68(4)	62(4)	29(3)	25(3)	-15(3)
C(33)	51(3)	38(3)	48(3)	6(2)	19(3)	-6(2)
C(34)	40(3)	25(2)	40(3)	3(2)	13(2)	-3(2)
C(35)	43(3)	30(2)	41(3)	-3(2)	14(2)	-6(2)
C(36)	51(3)	40(3)	56(3)	-9(2)	22(3)	0(2)
C(37)	69(4)	36(3)	50(3)	-5(2)	17(3)	-3(3)
C(38)	60(4)	38(3)	55(3)	-5(2)	6(3)	-17(3)
C(39)	41(3)	40(3)	60(3)	1(2)	13(3)	-9(2)
C(40)	36(2)	23(2)	47(3)	-1(2)	16(2)	2(2)
C(41)	51(3)	35(3)	57(3)	-12(2)	29(3)	-13(2)
C(42)	52(3)	42(3)	72(4)	-15(3)	27(3)	-18(2)
C(43)	50(3)	43(3)	64(4)	-14(3)	11(3)	-11(2)
C(44)	54(3)	48(3)	48(3)	0(2)	12(3)	1(3)
C(45)	45(3)	30(2)	52(3)	2(2)	22(2)	1(2)
C(46)	24(2)	31(2)	64(3)	-9(2)	19(2)	-5(2)
C(47)	42(3)	39(3)	71(4)	-12(3)	21(3)	-3(2)
C(48)	51(3)	43(3)	81(4)	-20(3)	17(3)	-11(3)
C(49)	42(3)	40(3)	102(5)	-29(3)	20(3)	-12(2)
C(50)	43(3)	26(3)	113(6)	-1(3)	21(3)	-2(2)
C(51)	31(2)	31(3)	78(4)	0(2)	16(3)	1(2)
C(52)	54(3)	27(2)	54(3)	-5(2)	25(3)	-16(2)
C(53)	72(4)	83(5)	65(4)	-18(4)	32(4)	19(4)
C(54)	93(6)	88(5)	46(4)	-17(3)	12(4)	31(4)
C(55)	58(4)	47(3)	53(3)	-8(3)	6(3)	-17(3)
C(56)	40(3)	92(5)	67(4)	22(4)	19(3)	-7(3)
C(57)	48(3)	103(5)	52(3)	22(3)	22(3)	-7(3)
C(58)	50(3)	28(2)	72(4)	2(2)	39(3)	3(2)
C(59)	71(4)	39(3)	75(4)	3(3)	49(3)	-7(3)
C(60)	74(4)	61(4)	86(5)	7(3)	58(4)	-10(3)
C(61)	69(4)	56(4)	71(4)	28(3)	49(3)	26(3)
C(62)	108(6)	38(3)	145(7)	-3(4)	97(6)	11(3)
C(63)	99(5)	35(3)	153(7)	-16(4)	96(6)	-11(3)
C(64)	44(3)	19(2)	58(3)	-6(2)	22(2)	-3(2)
C(65)	100(6)	76(5)	114(6)	50(4)	83(5)	55(4)
C(66)	114(6)	58(4)	101(5)	28(4)	81(5)	36(4)

C(67)	68(4)	30(3)	65(4)	5(3)	19(3)	-9(3)
C(68)	51(4)	51(4)	135(7)	46(4)	32(4)	5(3)
C(69)	41(3)	50(3)	120(6)	21(4)	43(4)	3(3)
P(1)	34(1)	27(1)	43(1)	4(1)	18(1)	-2(1)
P(2)	39(1)	24(1)	56(1)	-5(1)	26(1)	-4(1)

Table S6. Hydrogen coordinates ($\times 10^4$) and isotropic displacement parameters ($Å^2 \times 10^3$) for $\mathbf{1^+(CN)_2}$.

	x	y	z	U(eq)
H(6A)	8034	10361	1656	99
H(6B)	7547	9450	1712	99
H(6C)	7096	10292	1275	99
H(7A)	7988	10078	198	114
H(7B)	8455	10568	839	114
H(7C)	7520	10749	497	114
H(9)	5403	5587	596	52
H(10)	4330	6089	-269	56
H(11)	4351	7561	-673	52
H(12)	5427	8580	-238	49
H(15)	9521	5704	2686	80
H(16)	10732	6429	3250	93
H(17)	11010	7904	2933	96
H(18)	10024	8775	2212	77
H(6A1)	7770	10359	1272	99
H(6A2)	8550	9880	1750	99
H(6A3)	7697	9392	1589	99
H(7A1)	8620	9424	267	114
H(7A2)	8966	10122	833	114
H(7A3)	8088	10280	340	114
H(9A)	5253	5803	400	52
H(10A)	4286	6528	-439	54
H(11A)	4543	7993	-751	55
H(12A)	5747	8769	-257	49
H(15A)	9175	5252	2688	62
H(16A)	10503	5677	3223	75

H(17A)	10986	7112	3023	76
H(18A)	10141	8121	2290	69
H(23)	5895	-383	2730	58
H(24)	6323	-1719	3321	65
H(25)	6674	-1629	4373	61
H(26)	6630	-197	4833	58
H(27)	6195	1142	4245	49
H(29)	7040	698	2825	84
H(30)	7959	1244	2399	119
H(31)	7714	2605	1849	119
H(32)	6697	3580	1834	80
H(33)	5836	3126	2325	54
H(35)	4338	2508	3100	46
H(36)	4243	3800	3681	58
H(37)	5391	4569	4293	64
H(38)	6635	4059	4343	66
H(39)	6748	2773	3775	58
H(41)	4296	539	2987	54
H(42)	3073	102	2269	65
H(43)	2755	477	1255	66
H(44)	3633	1333	948	62
H(45)	4868	1794	1659	50
H(47)	1505	7518	1488	61
H(48)	1761	8899	2053	73
H(49)	1429	10325	1557	76
H(50)	864	10393	515	75
H(51)	574	9028	-61	57
H(53)	76	7111	-1103	85
H(54)	-1160	7490	-1823	95
H(55)	-2239	7720	-1544	68
H(56)	-2053	7907	-523	80
H(57)	-797	7596	216	80
H(59)	2093	8011	113	67
H(60)	2971	7672	-382	79
H(61)	2828	6317	-940	70
H(62)	1804	5290	-1018	99
H(63)	986	5563	-458	98
H(65)	-242	6508	865	102

H(66)	-104	5459	1640	95
H(67)	975	4450	1973	67
H(68)	1904	4461	1507	96
H(69)	1798	5540	748	81

NMR Spectra

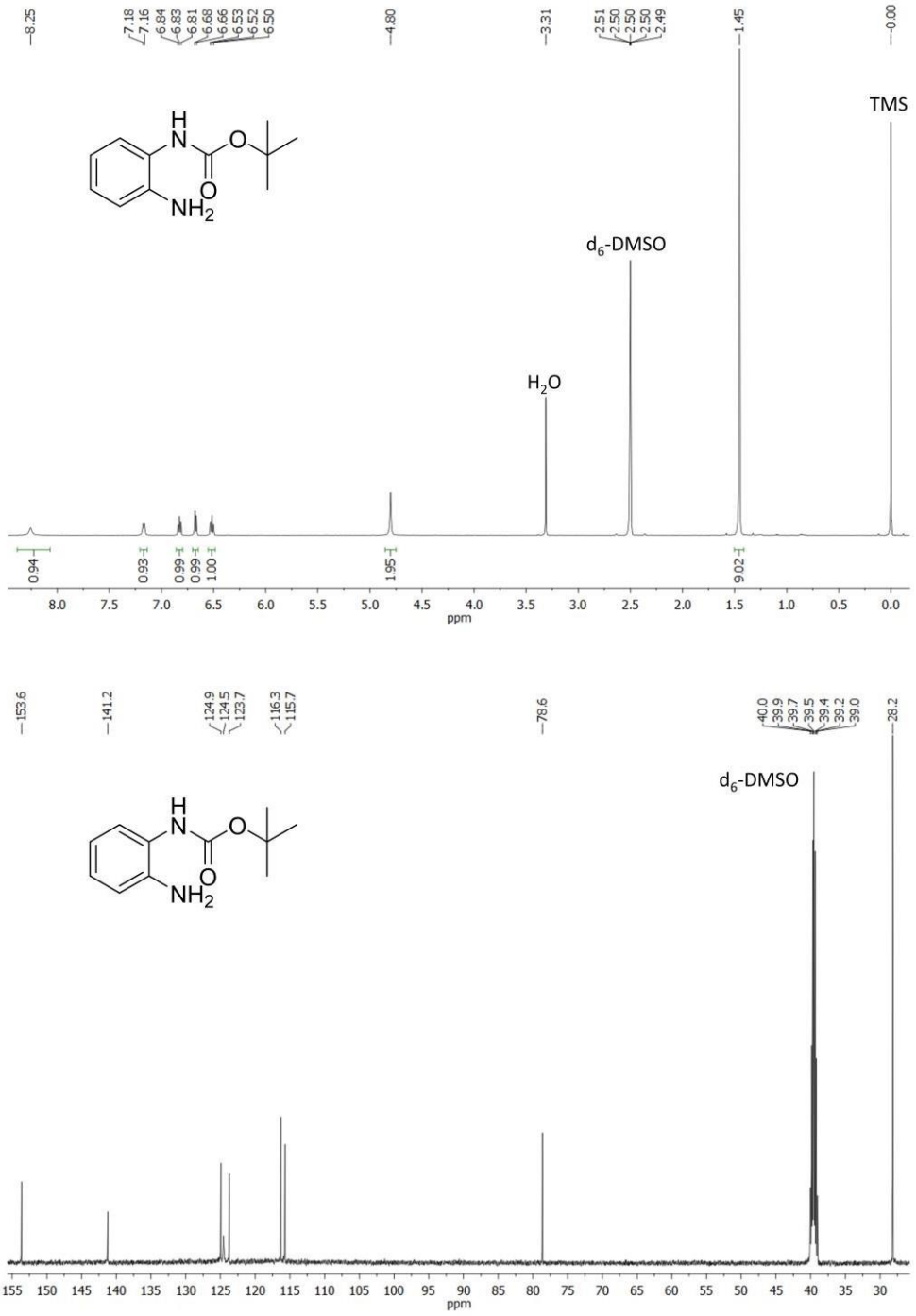

Fig. S20. The ^{1}H and ^{13}C NMR spectra of ligand precursor **A**.

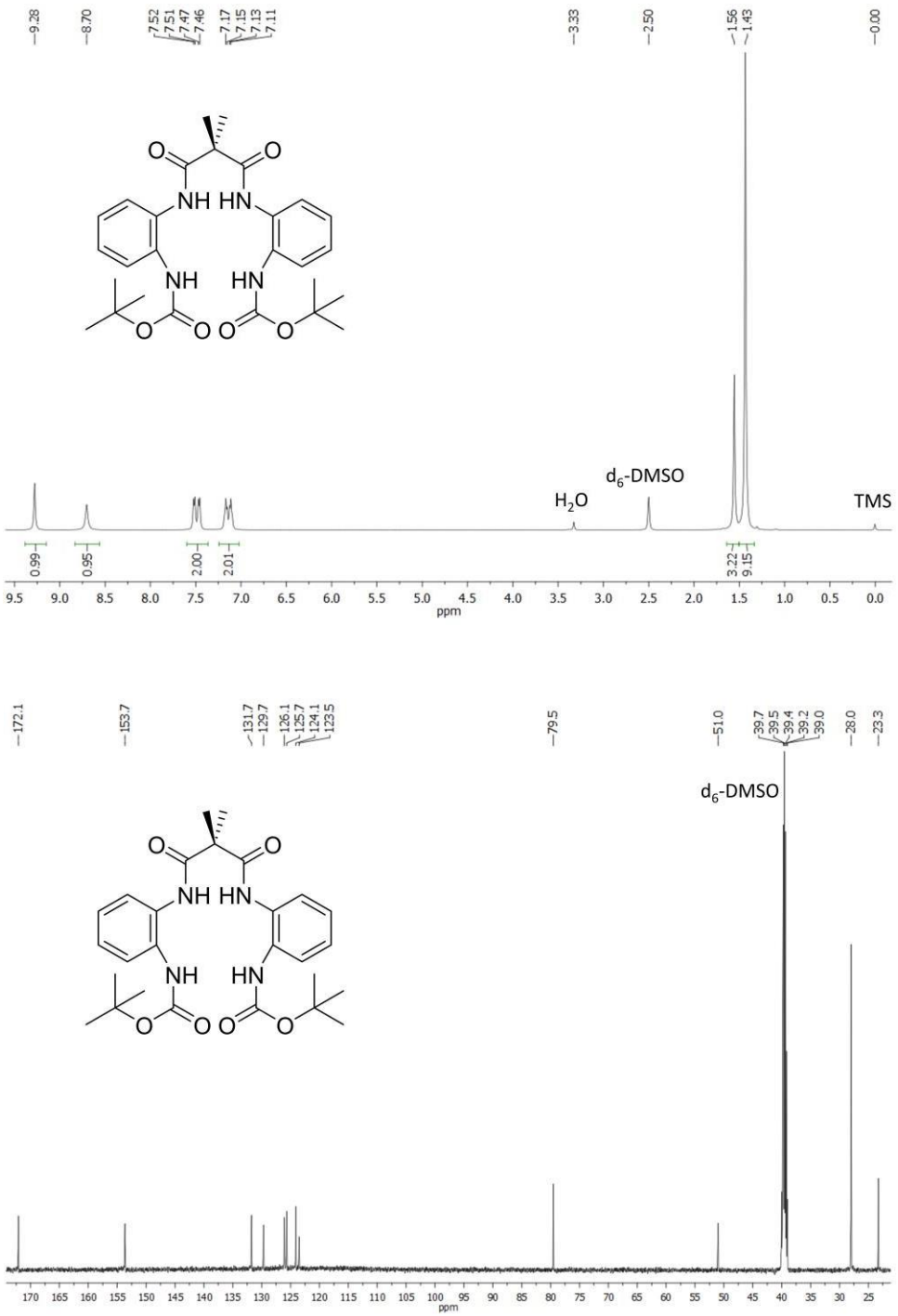

Fig. S21. The ^{1}H and ^{13}C NMR spectra of ligand precursor **B**.

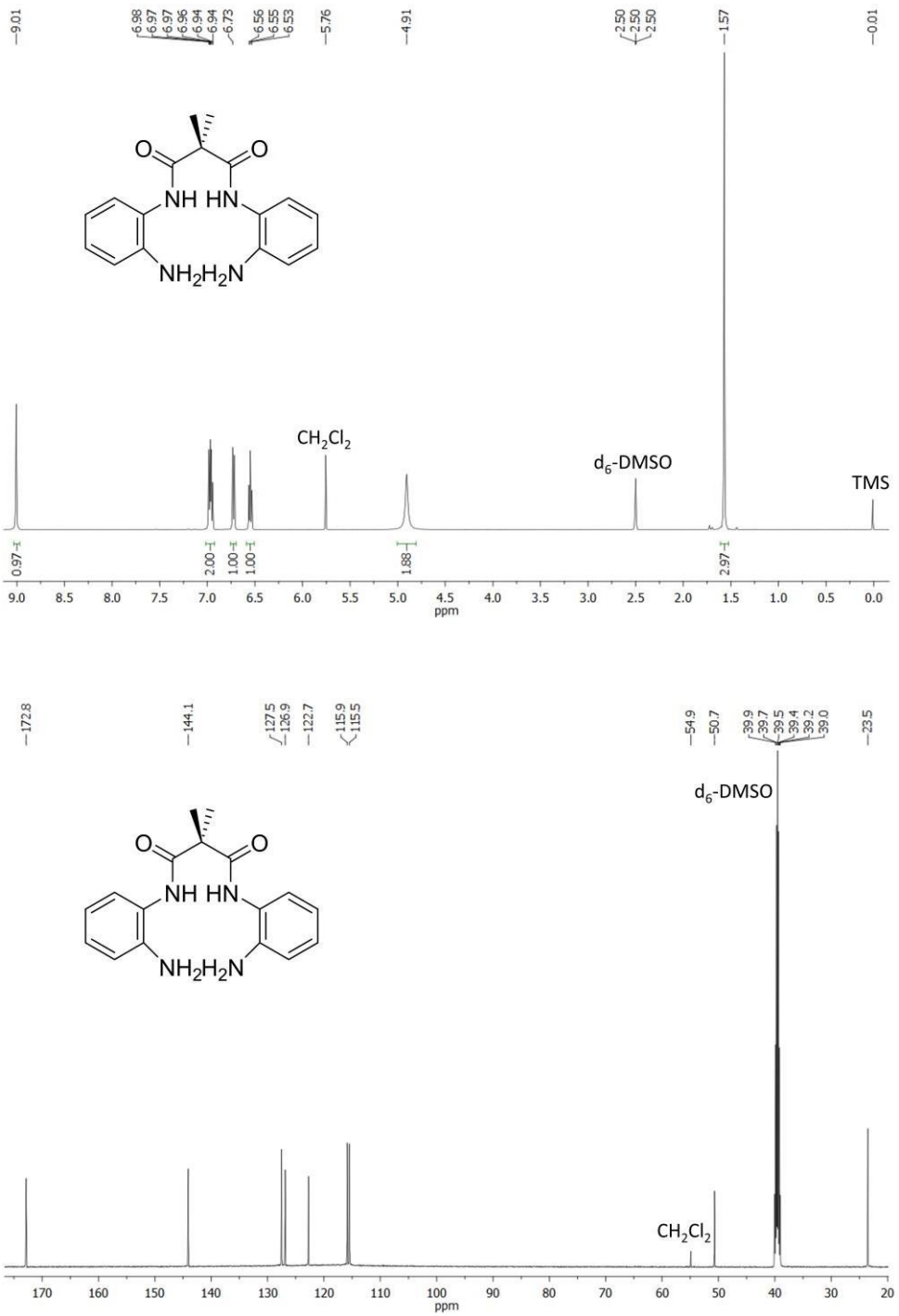

Fig. S22. The ^{1}H and ^{13}C NMR spectra of ligand precursor **C**.

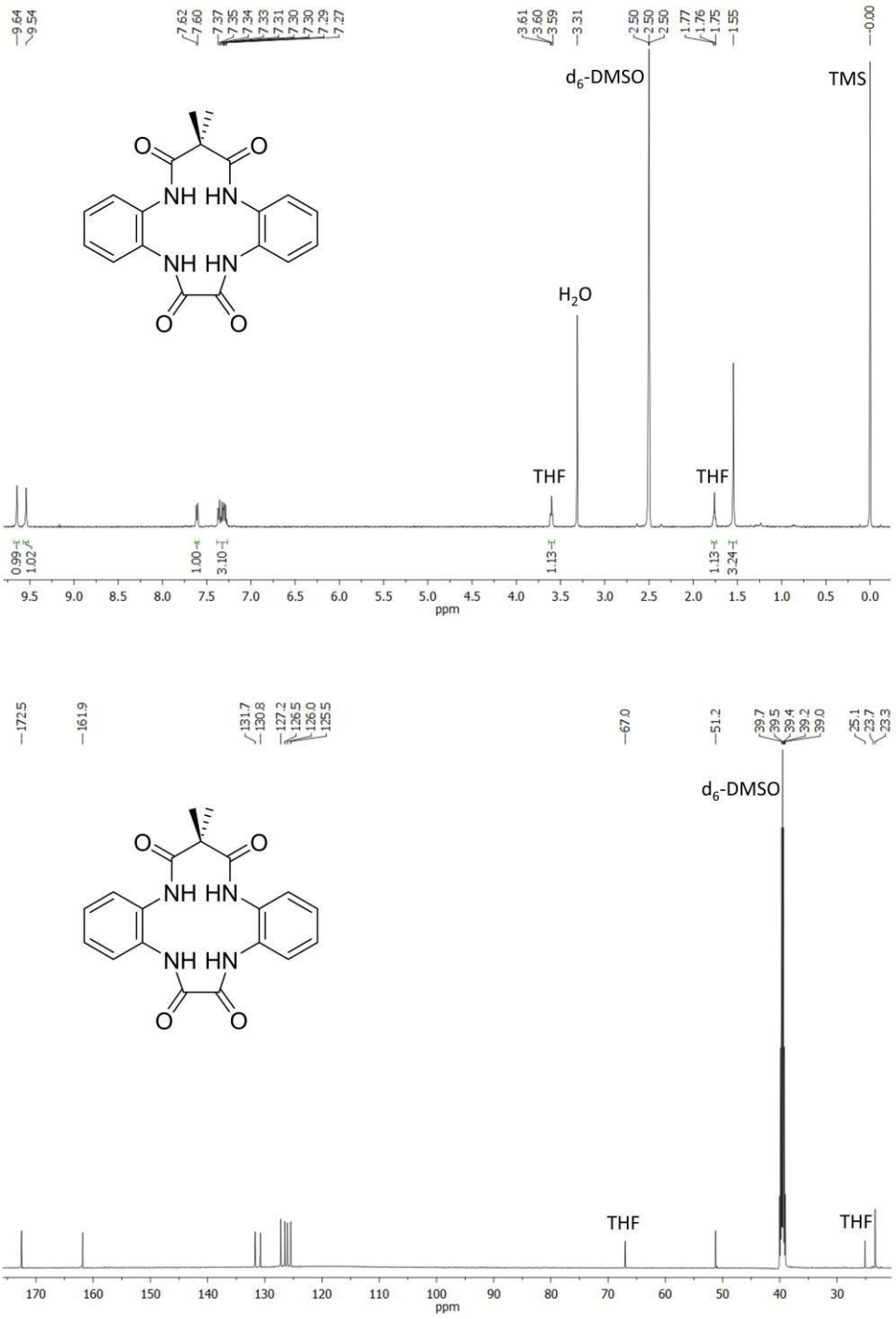

Fig. S23. The ^{1}H and ^{13}C NMR spectra of ligand precursor **D**.

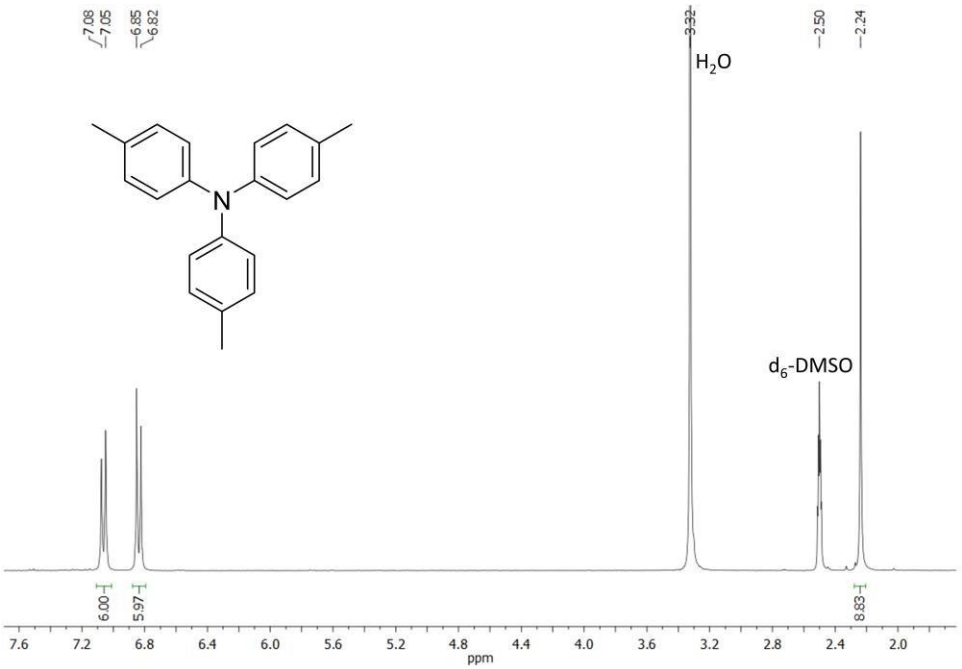

Fig. S24. The ^{1}H NMR spectrum of $(ArMe)_3N$.

References

1. W. C. Ellis, C. T. Tran, R. Roy, M. Rusten, A. Fischer, A. D. Ryabov, B. Blumberg and T. J. Collins, *J. Am. Chem. Soc.*, 2010, **132**, 9774-9781.
2. S. Z. Sullivan, A. Ghosh, A. S. Biris, S. Pulla, A. M. Brezden, S. L. Collom, R. M. Woods, P. Munshi, L. Schnackenberg, B. S. Pierce and G. K. Kannarpady, *Chem. Phys. Lett.*, 2010, **498**, 359-365.
3. G. Winter, D. W. Thompson and J. R. Loehe, in *Inorg. Synth.*, John Wiley & Sons, Inc., 2007, DOI: 10.1002/9780470132456.ch20, pp. 99-104.
4. A. Ghosh, A. D. Ryabov, S. M. Mayer, D. C. Horner, D. E. Prasuhn, S. Sen Gupta, L. Vuocolo, C. Culver, M. P. Hendrich, C. E. F. Rickard, R. E. Norman, C. P. Horwitz and T. J. Collins, *J. Am. Chem. Soc.*, 2003, **125**, 12378-12379.
5. M. J. Bartos, S. W. Gordon-Wylie, B. G. Fox, L. James Wright, S. T. Weintraub, K. E. Kauffmann, E. Münck, K. L. Kostka, E. S. Uffelman, C. E. F. Rickard, K. R. Noon and T. J. Collins, *Coord. Chem. Rev.*, 1998, **174**, 361-390.
6. A. Juris, V. Balzani, F. Barigelletti, S. Campagna, P. Belser and A. von Zelewsky, *Coord. Chem. Rev.*, 1988, **84**, 85-277.
7. H. S. Soo, A. Agiral, A. Bachmeier and H. Frei, *J. Am. Chem. Soc.*, 2012, **134**, 17104-17116.
8. A. Agiral, H. S. Soo and H. Frei, *Chem. Mater.*, 2013, **25**, 2264-2273.
9. E. Steckhan, in *Electrochemistry I*, ed. E. Steckhan, Springer Berlin Heidelberg, Berlin, Heidelberg, 1987, DOI: 10.1007/3-540-17871-6_11, pp. 1-69.
10. B. K. Bandlish and H. J. Shine, *J. Org. Chem.*, 1977, **42**, 561-563.
11. H. B. Goodbrand and N.-X. Hu, *J. Org. Chem.*, 1999, **64**, 670-674.